

Collision dynamics and entanglement generation of two initially independent and indistinguishable boson pairs in one-dimensional harmonic confinement

David I. H. Holdaway,^{*} Christoph Weiss, and Simon A. Gardiner*Joint Quantum Centre (JQC) Durham–Newcastle, Department of Physics, Durham University, Durham DH1 3LE, United Kingdom*

(Received 6 March 2013; published 26 April 2013)

We investigate finite-number effects in collisions between two states of an initially well-known number of identical bosons with contact interactions, oscillating in the presence of harmonic confinement in one dimension. We investigate two $N/2$ (interacting) ground states, which are initially displaced from the trap center, and the effects of varying interaction strength. The numerics focus on the simplest case of $N = 4$. In the noninteracting case, such a system would display periodic oscillation with a half harmonic oscillator period (due to the left-right symmetry). With the addition of contact interactions between the bosons, collisions generate entanglement between each of the states and distribute energy into other modes of the oscillator. We study the system numerically via an exact diagonalization of the Hamiltonian with a finite basis, investigating left-right number uncertainty as our primary measure of entanglement. Additionally, we study the time evolution and equilibration of the single-body von Neumann entropy for both the attractive and repulsive cases. We identify parameter regimes for which attractive interactions create behavior qualitatively different from that of repulsive interactions, due to the presence of bound states (quantum solitons), and explain the processes behind this.

DOI: [10.1103/PhysRevA.87.043632](https://doi.org/10.1103/PhysRevA.87.043632)

PACS number(s): 03.75.Lm, 05.45.Yv, 67.85.Bc

I. INTRODUCTION

Dilute gases of alkali-metal atoms have proved a powerful tool for the experimental investigation of quantum mechanical phenomena, from the level of single-atom physics up to mesoscopic levels via the creation of Bose-Einstein condensates (BECs) [1,2]. Much of the interest stems from the ability to experimentally realize many theoretically interesting potentials, such as optical lattices [3], double-well potentials [4], and periodic kicking [5], with the ability to control the effective dimensionality and interaction strength via Feshbach resonances. Another interesting property is the ability to support both bright and dark solitons [6,7].

Experimentally, it is possible to tune s -wave scattering lengths to both positive and negative values [8–10]. However, beyond a certain critical number (which is dependent on the trapping configuration and scattering length), the negative scattering length (attractively interacting) systems are unstable to collapse [11–14]. If trapping potentials are present in two spatial dimensions, attractive condensates can exhibit self-trapping, i.e., localization (at least in terms of pair-correlation functions) in a direction free of external potentials. In quasi-one-dimensional (quasi-1D) geometries, attractive BECs form bright matter-wave solitons with particlelike dynamics for the center of mass [15]. Parameter regimes for which systems are quasi-1D have been investigated via variational techniques [13], along with effective potential approximations to deal with residual 3D effects [16,17], leading to higher-order effective nonlinearities. In addition to this, bright gap solitons [18] have been created from repulsive atoms in optical lattices by exploiting anomalous dispersion to give the atoms a negative effective mass.

Negative scattering lengths also give interesting possibilities in double-well and lattice physics. Repulsive interactions between atoms are known to give rise to the famous Mott

insulator state [19], with a near-definite atom number per lattice site. If one has a definite number of atoms per site, there is effectively a total uncertainty in relative phase between lattice sites and thus no phase coherence. A measurement of relative phase should give totally random results and indeed this is what one finds when imaging the moment distribution of such a lattice: no distinguishable interference patterns. Attractive interactions could in theory be used to squeeze number statistics the opposite way such that the ground state would tend to a superposition of a quantum soliton (N -atom bound state) delocalized over every lattice site. When only two sites are present, such a state is referred to as a NOON state [20], which is useful for non-shot-noise-limited interferometry [21]. However, systems where the ground state is such a superposition are known to be extremely unstable to temperature, as phase differences between the two sites have almost no energy cost, thus typically replacing quantum uncertainty with statistical uncertainty. It is therefore preferable to create such states dynamically, for example, by splitting a moving quantum soliton [22,23], which has been achieved to some extent [24], but not in a low-energy regime.

Any closed quantum system with no decoherence effects will be described by a wave function that will evolve deterministically. As such the wave function at any point in time $|\psi(t)\rangle$ maps back to a unique $|\psi(0)\rangle$. Recent experiments have shown great possibility to observe this deterministic behavior in systems with a small number of cold atoms [25,26], with dynamics that can be analytically calculated and with precise tuning available in the scattering length and confinement potentials. Strongly correlated effects and quantum superpositions are generally much easier to achieve in few-body systems. Despite this, one can still envisage collective properties (such as expectation values of operators) of a time-dependent finite system tending to constant values when averaged over reasonable time scales or relaxation of local operators, as shown in [27]. Nonintegrable systems, upon coupling to another larger system, usually tend to an equilibrium configuration at long times, independently of the

^{*}d.i.h.holdaway@dur.ac.uk

initial state of either system (except for the total energy); however, recent theoretical observations have thrown doubt on this [28]. Additionally, when two coupled systems contain a similar number of elements the situation is less clear still. Our system is nonintegrable and contains two initially independent subsystems of the same size; hence we are interested to what extent equilibration occurs or where it is resisted. Quantum systems, for example, atoms populating sites in an optical lattice [29], are known to show partial revivals of the initial state in time, but are generally observed to show weaker revivals as time progresses in an apparent damping. We are interested in whether certain measures, specifically the number to the left and right of the trap center and the single-body von Neumann entropy, tend to constant values when averaged over sufficient time scales.

Entanglement between identical Bosons is not as easy to define as for nonidentical particles. One can consider a bipartite partitioning [30], which can be into sets of lower and more highly excited states or via states occupying separate regions of space, in our case the left and right of the center of mass. We wish to observe the generation of entanglement between initially independent systems develop over time. In the absence interactions, no real entanglement can be generated between the two subsystems (although our chosen measure is only meaningful when the subsystems are well separated). Additionally, with strong interactions the effect of the confinement may be diminished and the integrability of the free system [31] may also effect entanglement generation, particularly in the attractive case where a new length scale is introduced that can be smaller than the confinement [32].

The paper is organized as follows. Section II introduces the one-dimensional Hamiltonian and the unit rescaling to harmonic oscillator lengths, used throughout the paper. Next, the initial condition is introduced, with specific cases of interest mentioned. Section III discusses observables and measures of entanglement that we will use to investigate the system, including the variation in the number to either side of the trap center and the single-body von Neumann entropy. Section IV begins an analytic investigation of the system, focusing on the mechanisms by which interactions modify the dynamics of each displaced state and generate entanglement. Section V discusses a possible experimental realization of the system, using ultracold atoms in an optical lattice, with parameters discussed for cesium. Section VI contains a brief description of the numerical method, based on exact diagonalization. Section VII presents numerically obtained results for the evolution of our observables and entanglement measures in the system. Section VIII summarizes and concludes.

II. SYSTEM

A. Hamiltonian and unit rescaling

We consider an effective 1D system (taken to be reduced from a 3D configuration where the radial degrees of freedom are strongly confined by a harmonic trapping potential) of structureless bosons subject to attractive or repulsive contact interactions $V(|x_1 - x_2|) = g_{1D}\delta(x_1 - x_2)$, i.e., a Lieb-Liniger-(McGuire) gas [31–33], with the addition of an axial harmonic confining potential. In second-quantized form, this

can be described by the following Hamiltonian:

$$\hat{H} = \int dx \hat{\Psi}^\dagger(x) \left(-\frac{\hbar^2}{2M} \frac{\partial^2}{\partial x^2} + \frac{M\omega_x^2 x^2}{2} \right) \hat{\Psi}(x) + \frac{g_{1D}}{2} \int dx \hat{\Psi}^\dagger(x) \hat{\Psi}^\dagger(x) \hat{\Psi}(x) \hat{\Psi}(x), \quad (1)$$

where M is the mass and ω_x the axial (angular) trapping frequency; assuming a radial trapping frequency of ω_r , the coupling parameter $g_{1D} = 2\hbar\omega_r a_s$, with a_s the (3D) s -wave scattering length [34,35]. A satisfactory condition for this Hamiltonian to be valid is $N|a_s| \ll \sqrt{\hbar/M\omega_r}$ and $k_B T \ll \hbar\omega_r$, however it is likely to be still valid for $k_B T \sim \hbar\omega_r$, i.e., as long as thermal excitations are unlikely to significantly populate radial modes.

We use harmonic oscillator units (codified as $\hbar = \omega_x = M = 1$), meaning that length is in units of $\sqrt{\hbar/M\omega_x}$, time in units of $1/\omega_x$, and energy in units of $\hbar\omega_x$; a harmonic oscillator period is then 2π . The Hamiltonian rescales to

$$\hat{H} = \int dx \hat{\Psi}^\dagger(x) \left[-\frac{1}{2} \frac{\partial^2}{\partial x^2} + \frac{x^2}{2} + \frac{g}{2} \hat{\Psi}^\dagger(x) \hat{\Psi}(x) \right] \hat{\Psi}(x), \quad (2)$$

where $g = g_{1D}\sqrt{M/\hbar^3}\omega_x$ is the new dimensionless coupling parameter, which quantifies the relative strength of interaction.¹ In first quantization we can express this same Hamiltonian (for N particles) as

$$H(\vec{x}) = \sum_{k=1}^N \left(-\frac{1}{2} \frac{\partial^2}{\partial x_k^2} + \frac{x_k^2}{2} \right) + g \sum_{k=2}^N \sum_{j=1}^{k-1} \delta(x_k - x_j), \quad (3)$$

where x_k are the coordinates of the individual particles (generally considered to be ultracold atoms) and \vec{x} is a shorthand for the set of all N coordinates $\{x_1, x_2, \dots, x_N\}$. As the external potential is harmonic, $H(\vec{x})$ can be partitioned into two mutually commuting components [32], one describing the center of mass (giving rise to the Kohn mode [36]) and the other describing the remaining degrees of freedom. This separation can be exploited computationally, as the center-of-mass dynamics are those of a simple harmonic oscillator and therefore can be described exactly, reducing the effective dimensionality of the computational problem to $N - 1$.

B. Initial condition

1. General N -body case

We consider a highly non-mean-field-like initial condition, taking two $N/2$ -atom ground states (for a given g), equally and oppositely displaced from the trap center by a distance x_0 , and symmetrizing. The initial ($t = 0$) wave function is then

$$\psi(\vec{x}, 0) = \frac{B}{\sqrt{N!}} \sum_{\{\mathcal{P}\}} f^{(N/2)}(x_1 - x_0, \dots, x_{N/2} - x_0) \times f^{(N/2)}(x_{N/2+1} + x_0, \dots, x_N + x_0), \quad (4)$$

where $f^{(N/2)}(x_1, \dots, x_{N/2})$ is the ground state for $N/2$ atoms (generally numerically determined) in the harmonic trap, $\{\mathcal{P}\}$ is the set of all permutations of \vec{x} , and B is a normalizing

¹This relates to the parameter γ of [32] through $\gamma = [g(N - 1)]^{-2}$.

factor. Such an initial condition may be motivated by the idea of making two separate BECs and allowing them to collide within a harmonic trapping potential or from rapidly modifying a Mott insulator state in an optical lattice (as we will discuss in Sec. V). If the left and right components are well separated, i.e., the width of the atomic density distribution corresponding to $f^{(N/2)}$ is significantly less than x_0 , then there is a well-defined number of $N/2$ atoms on either side of the trap and left and right atoms are distinct by virtue of their position. Furthermore, as the center-of-mass dynamics are decoupled [32] and straightforward to determine, the dynamics experienced by an initial condition such as ψ can be readily extended to incorporate any initial condition for the center of mass, e.g., in particular, an overall oscillation about the trap center [15].

Conveniently, $\psi(\vec{x}, t)$ is in the ground state of the center-of-mass component of $H(\vec{x})$. To show this, we first define (unnormalized) Jacobi coordinates for a total of N identical particles. These consist of the center-of-mass coordinate

$$x_{C(N)} = \frac{1}{N} \sum_{k=1}^N x_k \quad (5)$$

and $N - 1$ further independent coordinates ξ_k (indexed by $k \in \{2, 3, \dots, N\}$), defined by

$$\xi_k = x_k - \frac{1}{k-1} \sum_{j=1}^{k-1} x_j. \quad (6)$$

Now using the Jacobi coordinates for $N/2$ particles and considering these $N/2$ particles in isolation, we can partition the $N/2$ -particle ground state into center-of-mass-dependent and -independent components $f^{(N/2)}(x_1, \dots, x_{N/2}) = \varphi(\xi_2, \dots, \xi_{N/2}) e^{-Nx_{C(N/2)}^2/4}$. Substituting Eq. (A1) into this expression, we can then define $\tilde{f}^{(N/2)}$ through

$$\begin{aligned} & f^{(N/2)}(x_1, \dots, x_{N/2}) \\ &= \varphi(\xi_2, \dots, \xi_{N/2}) \exp\left(\sum_{k=2}^{N/2} [(k-1)/2k] \xi_k^2 - \sum_{k=1}^{N/2} x_k^2/2\right) \\ &= \tilde{f}^{(N/2)}(x_1, \dots, x_{N/2}) \exp\left(-\sum_{k=1}^{N/2} x_k^2/2\right), \end{aligned} \quad (7)$$

where $\tilde{f}^{(N/2)}$ (as it can also be written as a function of $\{\xi_2, \xi_3, \dots, \xi_{N/2}\}$ only) is clearly independent of $x_{C(N/2)}$.

If we now expand to a full set of N coordinates, $\tilde{f}^{(N/2)}(x_1, \dots, x_{N/2})$ is also clearly independent of $x_{C(N)}$, as is (by symmetry) $\tilde{f}^{(N/2)}(x_{N/2+1}, \dots, x_N)$. Noting further that displacement by x_0 will not affect that part of $f^{(N/2)}$ independent of the center-of-mass coordinate, then for the identity permutation of ψ ,

$$\begin{aligned} & f^{(N/2)}(x_1 - x_0, \dots, x_{N/2} - x_0) f^{(N/2)} \\ & \quad \times (x_{N/2+1} + x_0, \dots, x_N + x_0) \\ &= \tilde{f}^{(N/2)}(x_1, \dots, x_{N/2}) \tilde{f}^{(N/2)}(x_{N/2+1}, \dots, x_N) \\ & \quad \times \exp\left[-\sum_{k=1}^N x_k^2/2 - x_0 \left(\sum_{k=N/2+1}^N x_k - \sum_{k=1}^{N/2} x_k\right) - Nx_0^2/2\right]. \end{aligned} \quad (8)$$

By the identities (A1) and (A7), the exponential reduces to $e^{-Nx_{C(N)}^2/2} \exp[-N(\sum_{k=N/2+1}^N \xi_k/k - x_0^2/2)]$, i.e., a term proportional to the center-of-mass ground state multiplied by a function of independent Jacobi coordinates. The identity permutation of ψ can thus be written as a product of the center-of-mass ground state and a function of the other independent Jacobi coordinates. This separation from the center-of-mass ground state occurs for every permutation of the coordinates x_k and so we conclude that the center-of-mass component of ψ is indeed in the ground state.

Taking a slightly different initial condition, when one combines ground states from two trapping potentials that are not equal to the final potential (with, e.g., tighter harmonic trapping), will introduce a breathing motion, which can still be considered separately from the remaining dynamics. It is also significant to note that the kind of initial condition we consider does not have a well-defined relative phase between the left and right components [37]. If a relative number uncertainty between left and right were to develop then this would no longer be the case and a meaningful relative phase could in principle be extracted.

2. Time evolution for the noninteracting case

If we take the case where $g = 0$, we can express the full time-dependent wave function [which we label $\psi_0(\vec{x}, t)$] analytically, as a symmetrizing product of two $N/2$ -atom product states

$$\psi_0(\vec{x}, t) = \frac{B_0}{\sqrt{N!}} \sum_{\{P\}} \prod_{k=1}^{N/2} \phi(x_k, -x_0, t) \prod_{j=N/2+1}^N \phi(x_j, x_0, t). \quad (9)$$

Here $\phi(x, \pm x_0, 0)$ is a Gaussian displaced by $\pm x_0$ from the trap center and [15,38]

$$\begin{aligned} \phi(x, x_0, t) &= \left(\frac{1}{\pi}\right)^{1/4} \exp\left(-\frac{[x - x_0 \cos(t)]^2}{2}\right) \\ & \quad \times \exp\{i[t/2 - x_0 \cos(t)x + x_0 \sin(2t)/4]\}, \end{aligned} \quad (10)$$

corresponding to an energy per particle of $E = (x_0^2 + 1)/2$, and the normalization constant $B_0 = 1 + \mathcal{O}(e^{-2x_0^2})$.

3. The $N = 4$ special case

If $N = 4$, the $f^{(2)}$ appearing in Eq. (4) are known analytically [39,40] and may, if $g < 0$, for sufficiently large g and x_0 , be considered to be bound-state dimers, held within an overall harmonic trapping potential. The general form is given by

$$\begin{aligned} f^{(2)}(x_1, x_2) &= \mathcal{N}U\left(-\nu, 1/2, \frac{[x_1 - x_2]^2}{2}\right) e^{-x_1^2/2} e^{-x_2^2/2} \\ &= \mathcal{N}U\left(-\nu, 1/2, \xi_2^2/2\right) e^{-\xi_2^2/4} e^{-x_{C(2)}^2}, \end{aligned} \quad (11)$$

with U Tricomi's confluent hypergeometric function, \mathcal{N} a normalization constant, and ν the effective quantum number (equal to zero for $g = 0$), as determined by the transcendental equation $\Gamma(1/2 - \nu)/\Gamma(-\nu) = -g/2^{3/2}$. This state has an energy of $2\nu + 1$, where there is a contribution of $1/2$ due to the center of mass. Equation (11) can then be inserted into

the initial condition

$$\psi(x_1, x_2, x_3, x_4, 0) = \frac{B}{\sqrt{4!}} \sum_{\{\mathcal{P}\}} f^{(2)}(x_1 - x_0, x_2 - x_0) \times f^{(2)}(x_3 + x_0, x_4 + x_0), \quad (12)$$

where $\{\mathcal{P}\}$ is the set of all $4!$ permutations of $\{x_1, x_2, x_3, x_4\}$. Note that, as $f^{(2)}(x_1, x_2) = f^{(2)}(x_2, x_1)$, the number of distinct permutations actually reduces to $4!/2!2! = 6$.

III. OBSERVABLES AND MEASURES OF ENTANGLEMENT

A. Left-right number

For our system, one useful measure to track the generation of entanglement is the variance in particle number to the left and right of the system's center of mass (which we will generally consider to be fixed at the origin). The initial condition we consider has $N/2$ atoms to either side with essentially no possibility of, say, $N/2 + 1$ to the right and $N/2 - 1$ to the left (probabilities for measuring such unequal partitionings decrease in a Gaussian manner with the initial separation). Hence the left- and right-particle-number variance will initially be zero. As the left and right particles approach and collide, all number partitionings become possible and so this measure is only informative when the particle density at the location of the center of mass is small.

We define a number-to-the-right operator

$$\hat{N}_R = \int_0^\infty dx \hat{\Psi}^\dagger(x) \hat{\Psi}(x) \quad (13)$$

[or in first quantization $\sum_{k=1}^N \Theta(x_k)$, where Θ is the Heaviside step function]; imaging one side of the trap would correspond to a projective measurement into the eigenstates of this operator, as is discussed in Sec. V. The expectation value of \hat{N}_R is the mean number of particles on the right-hand side: As the system is parity preserving, $\langle \hat{N}_R \rangle = N/2$ for all time for the initial conditions we consider.

The more informative number-to-the-right variance is

$$\Delta N_R = \langle \hat{N}_R^2 \rangle - \langle \hat{N}_R \rangle^2, \quad (14)$$

which, for our initial condition of two well-separated left and right components of definite number, should be approximately equal to zero. From Eq. (B6), the variance for a product state $\psi(\vec{x}) = \prod_{k=1}^N \phi(x_k)$ (symmetric about the trap center so that $\langle \hat{N}_R \rangle = N/2$) is

$$\Delta_P N_R = \langle \hat{N}_R \rangle (1 - \langle \hat{N}_R \rangle / N) = N/4, \quad (15)$$

which evaluates to unity if $N = 4$ (this is, however, the same as a symmetric superposition of one and three atoms to the right and left). It can also be shown (Appendix B 1) that for the case of $N = 4$ and no interactions ($g = 0$) [given by Eq. (9)], this variance evolves as

$$\Delta_P N_R = 1 - \text{erf}^2[x_0 \cos(t)] + \mathcal{O}(e^{-2x_0^2}), \quad (16)$$

with erf the error function.² Hence we have a function with period $T = \pi$, which is equal to unity when $t = (n + 1/2)\pi$ and vanishingly small in x_0 when $t = n\pi$.

In general, our wave function is not an eigenstate of \hat{N}_R and contains components of different \hat{N}_R eigenstates (for some given overall N , meaning that an additional specification of number-to-the-left operator eigenstates is not necessary). One can, however, calculate expectation values of operators defined over restricted regions of state space, specific to having exactly n (of N) atoms to the right of the trap center. An expectation value for an operator \hat{O} defined in this region is then

$$\begin{aligned} \langle \hat{O} \rangle_{n, N-n} &= \frac{\int_0^\infty dx_1 \cdots dx_n \int_{-\infty}^0 dx_{n+1} \cdots dx_N \psi^*(\vec{x}) \hat{O}(\vec{x}) \psi(\vec{x})}{P_{n, N-n}}, \end{aligned} \quad (17)$$

with

$$P_{n, N-n} = \int_0^\infty dx_1 \cdots dx_n \int_{-\infty}^0 dx_{n+1} \cdots dx_N |\psi(\vec{x})|^2 \quad (18)$$

the probability a perfect measurement of \hat{N}_R will find n of N atoms to the right (or, equivalently, $N - n$ to the left) of the trap center. This is equivalent to taking the usual expectation value over a new (normalized) wave function $\psi_{n, N-n}(\vec{x})$ defined by

$$\psi_{n, N-n}(\vec{x}) = \frac{\psi(\vec{x}) \sum_{\mathcal{P}} \prod_{k=1}^n \Theta(x_k) \prod_{j=n+1}^N \Theta(-x_j)}{\sqrt{P_{n, N-n} N! / n!(N-n)!}}, \quad (19)$$

where \mathcal{P} is the set of all unique permutations, of which there are $N! / n!(N-n)!$. Each such wave function is an eigenstate of \hat{N}_R , with eigenvalue n . In principle, one can partition the Hilbert space in such a way that it is the tensor product of a subspace describing only how many particles are to the left and right of the trap center and a subspace describing all other relevant properties of the system state. We may denote the set of eigenstates of \hat{N}_R spanning this number subspace by $\{|N - n, n\rangle\}$ such that

$$\hat{N}_R |N - n, n\rangle = n |N - n, n\rangle. \quad (20)$$

Further, it is also useful to consider distance-to-the-right and distance-to-the-right-squared operators, i.e.,

$$\hat{X}_R^{(j)} = \int_0^\infty dx x^j \hat{\Psi}^\dagger(x) \hat{\Psi}(x) \quad (21)$$

[given by $\sum_{k=1}^N \Theta(x_k) x_k^j$ in first quantization], for $j = 1, 2$. We denote the restricted (to having n of N atoms to the right of the trap center) expectation values of the position-to-the-right operator

$$R_{n, N-n}(t) = \langle \hat{X}_R^{(1)} \rangle_{n, N-n}. \quad (22)$$

These trace particlelike tracks, with widths around them described by

$$\sigma_{n, N-n}(t) = \sqrt{\langle \hat{X}_R^{(2)} \rangle_{n, N-n} - R_{n, N-n}^2(t)}. \quad (23)$$

²Satisfying $\text{erf}(0) = 0$ and $\text{erf}(\pm x) \rightarrow \pm[1 - \exp(-x^2)/\sqrt{\pi}x]$ as $x \rightarrow \infty$.

B. von Neumann entropy and relaxation

Averaging over all individual particles results in the single-body density matrix

$$\rho(x, x', t) = \langle \hat{\Psi}^\dagger(x') \hat{\Psi}(x) \rangle, \quad (24)$$

which is normalized to the total particle number N [$\int dx \rho(x, x, t) = N$]. From this, single-body properties of the many-body system may be determined, specifically the von Neumann entropy³

$$S_{\text{vN}}(t) = - \int dx \left(\frac{\rho(x, x, t)}{N} \right) \ln \left(\frac{\rho(x, x, t)}{N} \right). \quad (25)$$

Relaxation, in the sense of tending to states of higher entropy, is not present if the system is fully integrable, i.e., when $g = 0$, or if the trapping is removed and the eigenstates are given by the Bethe ansatz [31]. However, as the integrability is broken by the trapping, we expect some degree of thermalization due to (previously forbidden) mixing between states. It is of interest to determine how such thermalization time scales vary with the interaction strength and initial separations.

For a product state, ρ has a single nonzero eigenvalue of value N , meaning $S_{\text{vN}} \rightarrow 0$ (this is equivalent to a Bose-Einstein condensate being exactly described by a Gross-Pitaevskii wave function). A larger value of S_{vN} indicates occupancy of multiple eigenstates of ρ , equivalent to population of noncondensate modes due to thermal excitations or to quantum or dynamical depletion [42,43].

If the system equilibrates, S_{vN} will tend to a constant value. As our initial conditions result in repeated collisions at the trap center, the value of S_{vN} shows distinct oscillations that decay only slowly. We therefore also consider a time average over an oscillator period

$$\bar{S}_{\text{vN}}(t) = \frac{1}{2\pi} \int_t^{t+2\pi} dt' S_{\text{vN}}(t'), \quad (26)$$

along with its variance

$$\Delta \bar{S}_{\text{vN}}(t) = \int_t^{t+2\pi} dt' \left[\frac{S_{\text{vN}}(t')}{2\pi} - \bar{S}_{\text{vN}}(t) \right]^2. \quad (27)$$

If $S_{\text{vN}}(t)$ tends to a constant value, this will be shown by a relaxation of $\bar{S}_{\text{vN}}(t)$ to a constant value and a relaxation of $\Delta \bar{S}_{\text{vN}}(t)$ to 0, with the relaxation of $\bar{S}_{\text{vN}}(t)$ tending to occur on a significantly faster time scale than that of $\Delta \bar{S}_{\text{vN}}(t)$.

IV. ANALYSIS OF THE INTERACTING SYSTEM

A. Left-right separation of the Hamiltonian

As our initial condition consists of left and right components that are well separated and therefore distinguishable, we can initially treat the left and right components separately.

³This is sometimes referred to as the invariant correlation entropy [41] as it is independent of the basis chosen, at least up to truncation errors. Equation (25) is simply the position-representation rendering of $S_{\text{vN}} = -\text{Tr}[(\rho/N) \ln(\rho/N)]$, where the single-body density matrix ρ may of course be expressed in terms of any sufficiently complete basis (numerically, we employ the orthonormal Hermite functions and the trace becomes a sum of discrete diagonal matrix elements).

As these left and right clusters only interact for a short time during collisions in the center (so long as they stay as distinct clusters), it makes sense to treat interactions between these clusters perturbatively at early times. We therefore split the Hamiltonian into three, restricting the coordinates to the region $x_1 \leq x_2 \leq x_3 \leq x_4$, which is sufficient due to Bose symmetry. The three components are

$$\begin{aligned} H_L(x_1, x_2) &= \sum_{k=1}^2 \left(-\frac{1}{2} \frac{\partial^2}{\partial x_k^2} + \frac{x_k^2}{2} \right) + g\delta(x_2 - x_1), \\ H_R(x_3, x_4) &= \sum_{k=3}^4 \left(-\frac{1}{2} \frac{\partial^2}{\partial x_k^2} + \frac{x_k^2}{2} \right) + g\delta(x_4 - x_3), \\ H_I(x_2, x_3) &= g\delta(x_3 - x_2). \end{aligned} \quad (28)$$

The reason only adjacent interaction terms [$\delta(x_k - x_j)$ with $k - j = 1$] remain is that the other terms constitute a set of zero measure in the region we are considering, i.e., $x_1 = x_2$ occurs infinitely more often than $x_1 = x_3$, which necessarily implies $x_2 = x_3$ and so is a set of lower dimensionality. As [\hat{H}_L, \hat{H}_R] = 0, if we neglect \hat{H}_I our system can be described by a tensor product of the left and right components.⁴ Each Hamiltonian $\hat{H}_{L/R}$ can further be split into center-of-mass $\hat{H}_{L/R}^{(C)}$ and relative $\hat{H}_{L/R}^{(R)}$ parts, generating the dynamics of the left and right center-of-mass and relative coordinates [$x_{C(L)} = (x_1 + x_2)/2$, $x_{C(R)} = (x_3 + x_4)/2$, $x_{R(L)} = x_2 - x_1$, and $x_{R(R)} = x_4 - x_3$, respectively], which again mutually commute.

We consider the center-of-mass wave function of an n -atom cluster, which is a Gaussian displaced from the trap center by some value X_n . Without the influence of \hat{H}_I our system consists of two indistinguishable clusters (with internal degrees of freedom considered to be in the ground state) undergoing simple harmonic motion. The primary reason for separating the Hamiltonian in this way is that our initial condition is in the ground state of $\hat{H}_{L/R}^{(R)}$ and is a displaced ground state of $\hat{H}_{L/R}^{(C)}$, hence any change to these wave functions is an excitation of the system.

B. Perturbative introduction of H_I

1. Overview

We consider the effect of introducing the Hamiltonian H_I , from Eq. (28), to the system. We look at three notable effects: changes to the wave function describing the left-right separation of the clusters; changes to the internal degrees of freedom within the clusters to the left and right; and interactions transferring atoms from one side to the other, creating a symmetric superposition.

2. Intercluster wave-function changes and pseudoperiodicity

The center-of-mass wave functions of each side, described by $\hat{H}_L^{(C)} + \hat{H}_R^{(C)}$, can change so long as the *global* center-of-mass wave function remains constant. Such changes lead to

⁴Commuting Hamiltonians imply $\exp(-i[\hat{H}_L + \hat{H}_R]t)|\psi\rangle = \exp(-i\hat{H}_L t)|\psi_L\rangle \exp(-i\hat{H}_R t)|\psi_R\rangle$, i.e., the time-evolution operator can be separated.

entanglement between the left and right clusters. To see this we note initially that the two-cluster wave function could be written as a product of left and right sides

$$\psi_0(x_{C(L)}, x_{C(R)}) \propto e^{-[x_{C(L)} - x_0]^2} e^{-[x_{C(R)} + x_0]^2} + \mathcal{T}_{\text{perm}}, \quad (29)$$

with $\mathcal{T}_{\text{perm}}$ denoting the permutation of R and L . This can be written in such a way as to explicitly separate the global center of mass:

$$\begin{aligned} \psi_0(x_{C(L)}, x_{C(R)}) &= e^{-[x_{C(L)} + x_{C(R)}]^2/2} \\ &\times \left\{ e^{-[x_{C(L)} - x_{C(R)} - 2x_0]^2/2} + \mathcal{T}_{\text{perm}} \right\}. \end{aligned} \quad (30)$$

The first term describes the global center of mass and is therefore fixed; the latter term, however, will be modified by interactions. Any such change (other than modifying x_0 or multiplying by $\exp(ip[x_{C(L)} - x_{C(R)}])$, which are simply rescalings of the initial position and kinetic energy, respectively) means that there will be terms involving products of the form $x_{C(L)}x_{C(R)}$ such that the wave function cannot be separated, indicating entanglement between the left and right sides. Such entanglement is notable in the context of solitons in free space, as integrability means that collisions cannot create entanglement once the states are asymptotically separated, although higher-order nonlinearities can also lead to entanglement [44]. Additionally, during collisions with attractive (repulsive) interactions, each cluster will accelerate (decelerate), subsequently returning to near its initial velocity, leading to a pseudoperiodicity.

3. Intracluster wave-function changes

The internal degrees of freedom described by $\hat{H}_{L/R}^{(R)}$ are initially in the ground state. Interactions during collisions will introduce excitations, with the energy transferring from the center-of-mass energy of each cluster. By conservation of energy this must reduce the amplitude of the oscillation. Attractive interactions will suppress such excitations, as the energy separation between ground and first (even-parity) excited states is greater than the harmonic oscillator level spacing, whereas for repulsive interactions this gap will be smaller. Note that when highly excited modes of the relative degrees of freedom $x_{R(L)}, x_{R(R)}$ are populated, these will always have a significant occupation for both L and R . One expects a qualitative difference in behavior between the attractive and repulsive cases to occur when the change between the first and second relative excited states differs by an amount of order unity (in harmonic oscillator units $\hbar\omega_x$). We note that for strongly attractive interactions,⁵ when $x_0 < -g/4$, there is not enough energy to break the bound-state clusters, making the relative degrees of freedom effectively inaccessible, but this is beyond the scope of the present paper.

4. Left-right atom transfer

Finally, the interactions can transfer an atom from one side to the other, mixing to a set of states with a symmetric superposition of one and three atoms at either side of the trap

(and, ultimately, back from this to the original state). There cannot be significant transfer to a state where there is a cluster of four atoms in the ground state (apart from the center-of-mass degree of freedom) on one side and zero on the other side, due to the invariance of the center-of-mass wave function, unless the state has all four atoms directly at the trap center. The state satisfying this condition is the ground state of the system and so the only possible population is that present at $t = 0$. Note that excited states of this four-atom cluster do make up parts of the oscillating cluster states; it is simply a different basis to consider the system in terms of.

A feature that distinguishes this effect from intracluster excitations is the energy difference between the two configurations, denoted $\Delta E_{\text{int}} = E_{3,1} - E_{2,2}$. For $g < 0$ the ground state of a three-atom relative Hamiltonian (that part of the Hamiltonian independent of the center of mass) plus a single free atom is lower in energy than two sets of two atoms in their relative ground states. The opposite is true for $g > 0$, but the energy difference can only be of the order of the harmonic oscillator energy spacings and so suppression is unlikely unless x_0 is small. The energy difference ΔE_{int} can take a variety of values when intracluster states are excited, but in the interest of studying transfer interactions, we look at the energy difference between two isolated ground states of $N = 2$ atoms and $(N = 3)$ - and $(N = 1)$ -atom ground states. This can be estimated analytically in three limits:

$$\Delta E_{\text{int}} \sim \begin{cases} g/\sqrt{2\pi} & \text{if } |g| \ll 1 \\ 1 & \text{if } g \gg 1 \\ -g^2/2 - 7/12g^2 & \text{if } g \ll -1, \end{cases} \quad (31)$$

the approximations used being overlapping noninteracting ground states, effective fermionization [45] (Tonks gas), and bound-state clusters [33] with the first-order energy correction from the trapping potential [32], respectively. Numerically determined values of ΔE_{int} are shown in Fig. 1; this energy proves to be an important quantity in the next section (note that this does not include the energy from the momentum or displacement of the clusters). Viewed classically, this transfer interaction causes transfer to a state where the kinetic energy

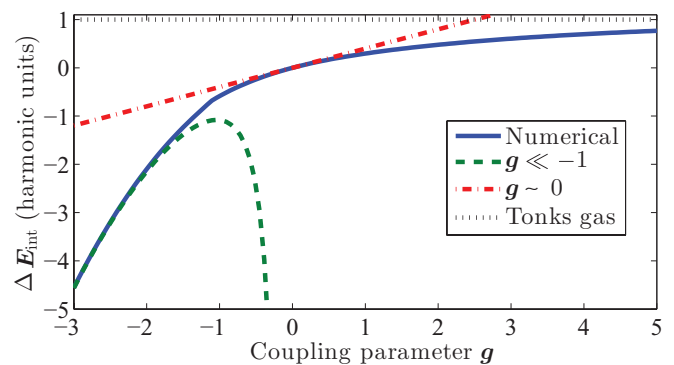


FIG. 1. (Color online) Energy difference $\Delta E_{\text{int}} = E_{3,1} - E_{2,2}$ between two-atom–two-atom and three-atom–one-atom ground-state clusters (in harmonic energy units $\hbar\omega$) as a function of the dimensionless coupling parameter g (quantifying the interaction strength). Analytic estimates from Eq. (31) are shown for comparison, with the Tonks gas being the $g \rightarrow \infty$ limit.

⁵In this regime energies scale as $-g^2n(n-1)/2$ for an n -atom ground state [33].

of the clusters was different from the original by an amount equal to ΔE_{int} , in order to conserve energy.

C. Mixing between different number configurations via time-dependent perturbation theory

We now investigate the atom transfer effect outlined in Sec. IV B4, predicted to be most significant for $g < 0$. We can write our wave function at any point in time as

$$|\psi(t)\rangle = c_{2,2}(t)|\psi_{2,2}(t)\rangle + c_{1,3}(t)|\psi_{1,3}(t)\rangle + c_{0,4}(t)|\psi_{0,4}(t)\rangle, \quad (32)$$

with $|\psi_{n,N-n}(t)\rangle$ normalized wave functions that are superpositions of states with n and $N - n$ atoms to the left, and vice versa, and $\{c_{n,N-n}\}$ a set of complex constants, the modulus squares of which are the probabilities to find n or $N - n$ atoms on either side. In order to qualitatively predict the incremental changes to $\{c_{n,N-n}(t)\}$ from before to after a collision, we use time-dependent perturbation theory, assuming $|g| \lesssim 1$ is a small parameter and neglecting any contribution from $c_{0,4}(t)$ (specifically at the time of collisions). We further assume that the center-of-mass motion of each $(n, N - n)$ -atom cluster in $|\psi_{3,1}(t)\rangle$ undergoes harmonic oscillation and is periodic in time with period $T = \pi$ and that any internal relative excitations in both $|\psi_{n,N-n}(t)\rangle$ are small compared to the ground state. This approximation is expected to work better for $g < 0$, for reasons outlined in Sec. IV B3, and at short times. As we initially have only $c_{2,2} \neq 0$, we assume $|c_{3,1}(t)| \ll |c_{2,2}(t)|$ as a regime of validity.

Formally, we perturb $\hat{H}_L + \hat{H}_R$ by \hat{H}_I [see Eq. (28)]. Our wave function

$$|\psi(t)\rangle \simeq c_{2,2}(t)|\psi_{2,2}(t)\rangle + c_{1,3}| \psi_{1,3}(t)\rangle \quad (33)$$

must solve

$$i \frac{d}{dt} |\psi(t)\rangle = [(\hat{H}_L + \hat{H}_R) + \hat{H}_I] |\psi(t)\rangle. \quad (34)$$

We assume that the difference between the time derivative of $|\psi_{2,2}(t)\rangle$ and $(\hat{H}_L + \hat{H}_R)|\psi_{2,2}(t)\rangle$ is small (which assumes that there is only a small amount of relative excitation) and neglect the time derivative of $|\psi_{3,1}(t)\rangle$; by our initial assumptions, the prefactor $c_{3,1}(t)$ is small. The time derivatives of $\{c_{n,N-n}(t)\}$ are thus given by

$$i[\dot{c}_{2,2}(t)|\psi_{2,2}(t)\rangle + \dot{c}_{3,1}(t)|\psi_{3,1}(t)\rangle] \simeq \hat{H}_I c_{2,2}(t)|\psi_{2,2}(t)\rangle. \quad (35)$$

Hence [using that $|\psi_{3,1}(t)\rangle$ and $|\psi_{2,2}(t)\rangle$ are orthogonal]

$$i\dot{c}_{2,2}(t) \simeq c_{2,2}(t)\langle\psi_{2,2}(t)|\hat{H}_I|\psi_{2,2}(t)\rangle, \quad (36)$$

$$i\dot{c}_{3,1}(t) \simeq c_{2,2}(t)\langle\psi_{3,1}(t)|\hat{H}_I|\psi_{2,2}(t)\rangle. \quad (37)$$

Within first-order perturbation theory, $\langle\psi_{2,2}(t)|\hat{H}_I|\psi_{2,2}(t)\rangle$ is periodic with a periodicity ($T = \pi$) half that of the oscillator period. The matrix element $\langle\psi_{3,1}(t)|\hat{H}_I|\psi_{2,2}(t)\rangle$ is a product of a function with period $T = \pi$ and the complex exponential $\exp(-i\Delta E_{\text{int}}t)$ of the energy difference between the intracluster degrees of freedom in both configurations (as plotted in Fig. 1).

Denoting the periodic component of the interaction terms $\langle\psi_{n,N-n}(t)|\hat{H}_I|\psi_{2,2}(t)\rangle$ as $f_{n,N-n}(t)$, we must therefore

solve

$$i\dot{c}_{2,2}(t) \simeq c_{2,2}(t)g f_{2,2}(t), \quad (38)$$

$$i\dot{c}_{3,1}(t) \simeq c_{2,2}(t)g f_{3,1}(t) \exp(-i\Delta E_{\text{int}}t), \quad (39)$$

with the boundary condition $c_{2,2}(0) = 1$. We first assume that the initial separation x_0 and the coupling magnitude $|g|$ are not large. Within this regime we assume that we can approximate $f(t)$ by a first-order Fourier series $f(t) \approx 1 - \cos(2t)$, which implies that all $f_{n,N-n}(t)$ differ only by a constant value; hence $f_{n,N-n}(t) = Af(t)$ and $f_{1,3}(t) = Bf(t)$, with A and B dependent in principle on g and quite heavily on x_0 . We can use this to solve Eq. (39),

$$c_{2,2}(t) \simeq \exp\left(i \int_0^t dt' Ag f(t')\right) \simeq \exp\{i Ag [t - \sin(2t)/2 + \dots]\}, \quad (40)$$

and if we neglect ΔE_{int} under the assumption that the relative energy on both sides is similar,

$$c_{3,1}(t) \simeq \frac{B}{A} \left[\exp\left(igA \int_0^t dt' f(t')\right) - 1 \right]. \quad (41)$$

For short times, we can expand $c_{3,1}(t) \approx B[igt + \mathcal{O}(g^2t^2, g \cos(2t))]$, i.e., proportional to gt and oscillatory terms and hence giving a linear increase when $t = n\pi$. At longer times the phase evolution of $c_{2,2}(t)$ becomes important, leading to cancellation in the terms of $c_{3,1}(t)$ and giving oscillatory behavior with a period dependent on g . The linear increase with g after a collision is not expected to continue when $g \gtrsim 1$ as higher-order terms become increasingly important and the perturbation theory breaks down.

We have so far neglected the difference in internal energy. This will introduce an additional phase between $c_{3,1}(t)$ and $c_{2,2}(t)$. With this included we have

$$c_{3,1}(t) \simeq \int_0^t dt' [igBc_{2,2}(t')f(t') \exp(-i\Delta E_{\text{int}}t')] \simeq igB \int_0^t dt' f(t') \exp(i[Ag - \Delta E_{\text{int}}t' - \mathcal{T}_{\text{osc}}]), \quad (42)$$

with \mathcal{T}_{osc} denoting oscillatory terms such as $k \cos(2t)$, which are periodic with $t \rightarrow t + \pi$ or shorter fractions of π for the higher-order terms. Summing together terms of different phases will produce cancellation, hence if the $\exp(i[Ag - \Delta E_{\text{int}}t])$ term has the same periodicity as $f(t)$ and the \mathcal{T}_{osc} terms, both π , the overall increase will be linear in time with no higher-order polynomial terms. This could therefore lead to resonant (suppressed) transfer if $Ag - \Delta E_{\text{int}} \approx n$ with n even (odd) and slightly suppressed transfer if n is a rational number not close to an even integer, e.g., $1/2, 1/3, 3/2$. As noted earlier, the $g \rightarrow \infty$ limit gives $\Delta E_{\text{int}} \sim 1$ and thus should lead to suppressed transfer if $|Ag| \lesssim 1/2$. We note that when $|g| \sim 0$ this resonance condition appears to be matched up to a factor $g[A - (2\pi)^{-2}]$, giving very long cancellation periods; however, as we see in Fig. 4 (and by the fact the perturbation strength scales proportionally to g), the rate of atom transfer scales proportionally to g and so cancellation can still occur before a significant population transfer is achieved.

This simple analysis neglects higher-order effects such as pseudoperiodicity, and intracluster excited states are not treated explicitly. However, qualitatively we expect an initially

weak linear increase with long-time oscillation effects for small $|g|$, and for $g \gtrsim 1$ the time scale of these oscillations should drop.

D. Amplitude bound to oscillations

One can look at each left-right number eigenstate [Eq. (20)] separately, assuming that we have a probability of p for $|2, 2\rangle$ and of $(1-p)/2$ for $|3, 1\rangle$ (with the same for the $|1, 3\rangle$ state), no occupation of $|4, 0\rangle$ or $|0, 4\rangle$, and there is no overlap between the states and no mixing via the Hamiltonian. We can then state the energy $E_{1,3} = \langle 1, 3 | \hat{H} | 1, 3 \rangle$ as

$$E_{1,3} = E_{\text{pot},1} + E_{\text{pot},3} + E_{\text{kin},1} + E_{\text{kin},3} + E_{\text{int},3}. \quad (43)$$

Each term in this equation refers to the kinetic, potential, and interaction energy of each side, with one or three atoms, respectively (note that there is no interaction energy for the single-atom side, taken without loss of generality as being left). Noting that the kinetic and potential energy terms must be positive, we can derive the inequality

$$E_{\text{pot},1} \leq E_{1,3} - (E_{\text{kin},3} + E_{\text{int},3}). \quad (44)$$

Using the conservation of $E = \langle \hat{H} \rangle$ and $\Delta E^2 = \langle \hat{H}^2 \rangle - E^2$, it can be shown that (see Appendix D)

$$|E_{3,1} - E| \leq \sqrt{\frac{p}{1-p}} \Delta E, \quad (45)$$

which is equivalent to

$$E - \sqrt{\frac{p}{1-p}} \Delta E \leq E_{3,1} \leq E + \sqrt{\frac{p}{1-p}} \Delta E. \quad (46)$$

Combining the upper bound of the above equation with Eq. (44), we obtain

$$E_{\text{pot},1} \leq \left(E + \sqrt{\frac{p}{1-p}} \Delta E \right) - (E_{\text{kin},3} + E_{\text{int},3}). \quad (47)$$

Finally, noting that $E_{\text{pot},1} = \langle x^2 \rangle_1 / 2 \geq \langle x \rangle_1^2 / 2$, with $\langle \hat{O} \rangle_1$ meaning the expectation value of the one-particle side of the wave function, we can obtain an inequality for the one-atom position expectation value

$$\langle x \rangle_1 \leq \sqrt{2} \sqrt{\left(E + \sqrt{\frac{p}{1-p}} \Delta E \right) - E_{\text{int},3}}. \quad (48)$$

We can see that larger, positive g will constrain this bound, up to a point of saturation at the Tonks-gas limit, whereas potentially it is unbounded as $g \rightarrow -\infty$ (energies in this regime scale proportionally to $-g^2$ [33]) as the atoms gain a large amount of energy.

V. POSSIBLE EXPERIMENTAL REALIZATION OF THE FOUR-ATOM SYSTEM

A. Optical lattice scheme

Our results could be tested by creating an optical superlattice [46] of two overlapping lattices, with one double the frequency of the other, and then loading this with two atoms per site (in the ground state) in a Mott insulator regime

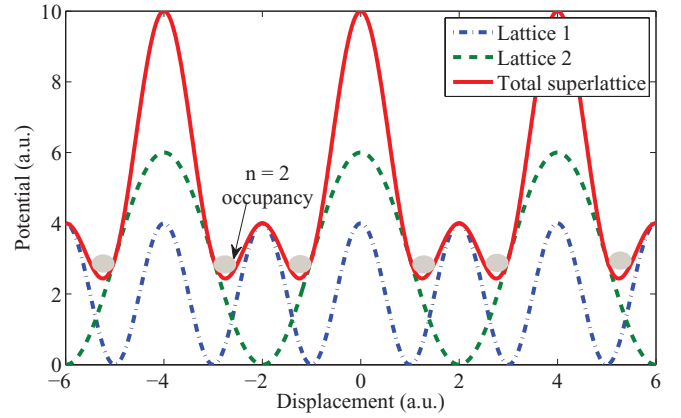


FIG. 2. (Color online) Schematic potential from an optical superlattice created by overlapping two lattices (all units are arbitrary). Gray circles represent a loading of two atoms in the ground state of each well. Our suggested scheme tunes the interactions to the desired value and then turns off the double-frequency (dotted line) lattice, leaving only the broader lattice (dot-dashed line), after which the atomic dimers collide.

[47]. This is shown schematically in Fig. 2. The interactions could then be tuned to be attractive via a magnetic Feshbach resonance at such a rate that tunneling between sites is small, but the two atoms on each site tend to the ground state given by Eq. (11). The double-frequency lattice could then be ramped down, leaving only the wider lattice, thus creating the initial conditions of two equally separated dimers in an approximately harmonic potential.

Some freedom with x_0 could be achieved by modifying the relative strength of the double-frequency lattice compared with the primary lattice. Reducing it will push the minimum closer together, but also make tunneling between the sites more significant. Careful ramping-down schemes of the laser power of the double-frequency lattice could also be incorporated, which would give further freedom to move the sites closer together after creating the dimers. Slower ramping will also make things closer to adiabatic, thus reducing the excitation in each dimer created by the switch off. The relative velocity between the two dimers in terms of the final harmonic oscillator units will equate to an effective initial separation: approximately the separation the dimers will reach after the first collision. A faster (slower) ramping scheme would give a larger (smaller) effective x_0 ; however, to be most applicable to the results of this paper, a slow scheme would be ideal to minimize excitations and minimize the degree of anharmonicity in the potential that the dimers sample.

After some free-evolution time, the double-frequency lattice could then be quickly restored with an extremely high lattice depth, separating the left and right components of the wave function, with no further tunneling possible. This would allow for a direct measurement of \hat{N}_R as defined in Eq. (13), by then imaging the lattice with resonant light; light-induced collisions [48] will reduce this to a parity measurement with an empty site being either a zero or two population and a single atom being a one or three population. This is actually sufficient information, assuming that we know the total atom number in the two sites was exactly 4. In terms of the states given in Eq. (20), no atoms on either site is a measurement of a

$|2,2\rangle$ configuration (or a $|4,0\rangle$ and $|0,4\rangle$ configuration, but this is only significant during collisions), both sites occupied is a measurement of a $|3,1\rangle$ and $|1,3\rangle$ configuration, and a single occupied site and an empty site would imply that some inelastic process has occurred (such as three-body recombination or background gas collisions) and such a result would thus be null.

If the effective x_0 were an appreciable fraction of the lattice width, this scheme could also show some more interesting physics beyond the scope of this paper, with collisions coupling energy into the center-of-mass mode and the tunneling of the single atom in the single-trimer states (considered in Sec. IV C) to adjacent lattice sites. It could even have a kinetic energy greater than the maximum barrier height between sites and join an effective conduction band [49], allowing for entanglement between lattice sites. These effects may also be worthy of experimental investigation.

B. Experimental parameters

In terms of typical experimental parameters, the s -wave scattering lengths would need to be very substantial in order to give measurable effects. Strong interactions generally require tuning scattering lengths near Feshbach resonances, and in such strongly interacting regimes confinement effects can shift the effective 1D scattering length if a_s/a_\perp is not small [35]. The chosen Feshbach resonance would ideally be broad, minimizing uncertainty in the effective interaction associated with a lack of precise control of magnetic field fluctuations.

Alternatively, some atoms such as cesium can have large background scattering lengths far from resonances [50], e.g., $a_s \sim \pm 3000a_0$, where $a_0 \approx 5.3 \times 10^{-11}$ m is the Bohr radius. In terms of a rescaled g parameter in harmonic oscillator units, if we have $\omega_x \sim 2\pi \times 1$ Hz and very strong radial confinement $\omega_r \sim 2\pi \times 0.4$ kHz, we have

$$g = 2\omega_r a_s \sqrt{\frac{m}{\hbar\omega_x}} \sim \pm 1.2, \quad (49)$$

which is of unitary order.

We essentially have three experimentally tunable parameters a_s , ω_x , and ω_r , which can be varied smoothly with small adjustments to a magnetic field or modifying laser powers, focusing, or detunings. However, dropping ω_x is undesirable as it increases experimental time scales and increases the likelihood of background gas collisions; additionally, unwanted three-body recombination effects scale proportionally to $|a_s|^4$ (generally being worse for $a_s < 0$), meaning one would need to determine an appropriate compromise solution.

VI. NUMERICAL METHOD

A. Basis-set expansion

To perform many-body computations we expand the field operator over the set of Hermite functions of a given width W ,

$$\varphi_k(Wx) = \sqrt{\frac{W}{k!2^k\pi^{1/2}}} H_k(Wx) \exp(-W^2x^2/2), \quad (50)$$

with $H_k(x)$ the Hermite polynomials, and diagonalize the Hamiltonian in a Fock state basis $|n_0, \dots, n_\infty\rangle$, truncated via the condition $\sum_k kn_k \leq \eta$. Such a calculation would require an unfeasible amount of states to converge were it not for the

fact that the center-of-mass part of the Hamiltonian commutes with the rest of it. This means that we can just consider a subset of this truncated Fock space where the center of mass of the gas is in the same state. This does not have to be the ground state, as we simply ignore the center-of-mass time evolution and can account for it later. The procedure essentially involves diagonalizing the finite basis in terms of the operator

$$\hat{A}^\dagger \hat{A} = \sum_{k,j} \sqrt{(k+1)(j+1)} \hat{a}_{k+1}^\dagger \hat{a}_k \hat{a}_j^\dagger \hat{a}_{j+1} \quad (51)$$

(where $\hat{A}^\dagger = \sum_k \sqrt{k+1} \hat{a}_{k+1}^\dagger \hat{a}_k$ is the creation operator for a dipole mode of width W) and taking the eigenvectors with eigenvalue zero; this procedure is discussed in detail in [32]. For the calculations in this paper we use the eigenstate width $W = 1$ as the harmonic oscillator length is always a relevant scale.

B. Convergence testing

We first need to represent our initial condition in terms of this basis set, noting that due to the truncation the state cannot be represented exactly, with larger initial displacements and larger coupling magnitudes g harder to represent in this basis. We require a reasonable fidelity of our numerical initial condition to the true state, achieving fidelities greater than 99.5% for all the numerics used in this paper.

Measuring convergence during time evolution with such a method is more difficult. Performing the calculations with a variety of basis sizes and calculating the fidelity over time can give an indication for how long the calculations are reliable, for which we plot, in Fig. 3, our most extreme values of g . This is probably the strictest measure of convergence applicable, given the large number of degrees of freedom in a many-body wave function, for example, a product state with a large number of atoms would have a fidelity exponentially tending to zero for any finite difference in the product wave function.

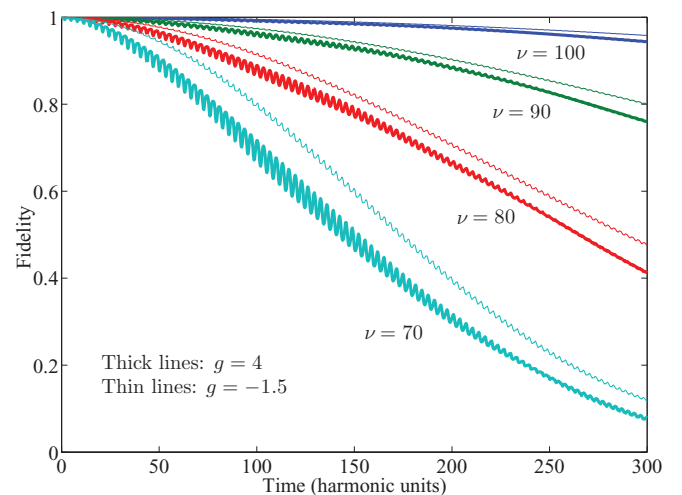


FIG. 3. (Color online) Plots of $|\langle \psi(\nu, t) | \psi(\nu_{\max}, t) \rangle|^2$, the fidelity of the wave function computed with smaller basis (energy cutoff at ν) to the wave function computed using a larger basis truncated at $\nu_{\max} = 113$. We have displayed results for the extreme values of g (in harmonic oscillator units) employed in the numerics: When lower absolute values of g are considered, the fidelity converges more rapidly with increasing ν .

VII. NUMERICAL RESULTS

A. Preamble

All the results graphed here are calculated for $N = 4$ and $x_0 = 3$ in order to investigate the effects of varying the strength of interaction (by varying the coupling parameter g) for small numbers. In general, smaller x_0 greatly increases interaction times between clusters and thus rates of atom transfer. It also reduces the amount of free energy in the system; however, a greater amount of the wave function will be found towards the center at all times and thus expectation values of \hat{N}_R will be harder to interpret. The results here are broken down into three sections: The first examines the variation in left-right number, the second examines the variance in position about one side, and the final section examines the single-body von Neumann entropy.

B. Left-right particle number dynamics

Because our initial condition has a definite number of two atoms on either side of the trap, the left-right number uncertainty ΔN_R in our system is initially very near zero. We note that a mean-field-like state or a symmetric superposition of one and three atoms on either side both give $\Delta N_R = 1$, which is also the value this quantity will take in our noninteracting system when each of the clusters collide. We therefore first consider the minimum-to-minimum values taken by ΔN_R before and after each collision. The change after the first collision is given in Fig. 4 and the change over the first

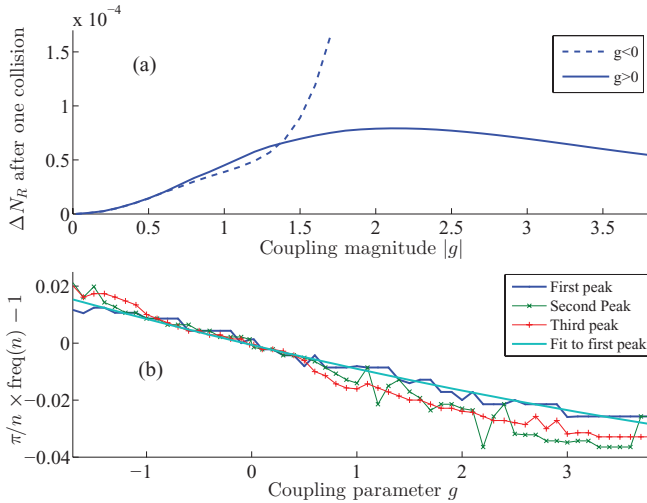


FIG. 4. (Color online) (a) Minimum value taken by ΔN_R [Eq. (B6)], after one collision. (b) Frequency difference (in harmonic units ω) of peaks in the Fourier transform of ΔN_R from the noninteracting values ($t = n\pi$) divided by n . (a) For $g > 0$, the increase to number uncertainty is greatest for $g \approx 2.3$ and decreases when the interaction strength is increased further. The $g < 0$ behavior is initially similar, but deviates at around $|g| = 0.6$; rather than saturating, it appears to increase even more rapidly with $|g|$. It is not clear what will happen for $g < 0$ and $|g| \gg 1$, which will be a topic for further investigation. (b) Existence of pseudoperiodicity in the system (in addition to low-frequency components relating to the long-time behavior). The noninteracting system has frequency peaks at $f_n = n/\pi$; the quadratic fit (solid line) indicates that these peaks shift by an amount roughly equal to $-ng/100\pi$.

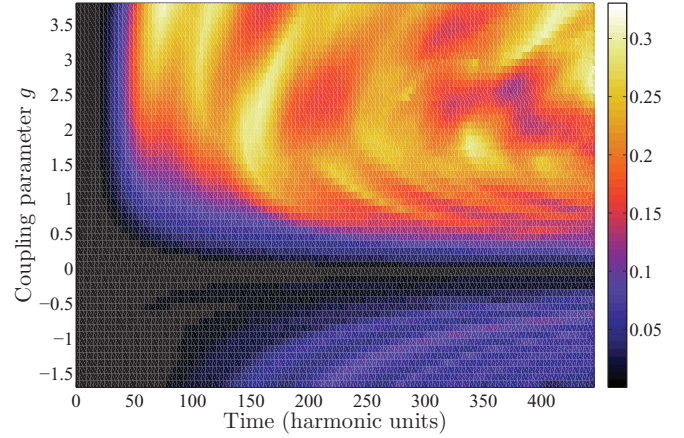


FIG. 5. (Color online) Minimum value obtained by ΔN_R , as given by Eq. (B6), after a given collision. For weak interactions ($|g| < 0.1$) the behavior is the same for attractive and repulsive, but for slightly larger values of g there is a clear difference in the time scales (measured in harmonic units ω^{-1}), with repulsive interactions producing larger number uncertainties more quickly, despite the fact that Fig. 4 shows that there is little difference in ΔN_R after one collision. This difference is likely due to the increased (decreased) energy spacing between the ground and first excited states of the two-atom system with attractive (repulsive) interactions, discussed in Sec. IV B3, and the energy difference between the two-two and three-one number configurations, as discussed in Sec. IV C, which leads to a phase mismatch. For large repulsive values ($g > 2$), ΔN_R reaches a maximum value and then undergoes complex partial revivals on time scales of 30 time units (tens of collisions).

150 collisions is plotted in Fig. 5. Despite the fact that the increase after the first collision is similar for both attractive and repulsive interactions of similar magnitude, the long-time change is very different, with the time scales being much longer in the attractive case.

In either case, the left-right number does not reach an equilibrium on the time scales considered, with oscillations and revivals present. The time-dependent perturbation theory of Sec. IV C indicates that atom transfer processes are suppressed by an internal energy difference between the $|2,2\rangle$ and $|3,1\rangle$ configurations of the wave function, which leads to destructive mixing over a few collisions, unless a phase-matching condition occurs. If intracluster excited states (discussed in Sec. IV B3) are present, the energy difference between each configuration ΔE_{rel} may be small (along with Ag), meaning cancellation occurs on longer time scales, leading to fluctuations in ΔN_R over 10 s of harmonic oscillator periods.

Figures 6 and 7(a) show the amplitude of each number component in the wave function as it evolves in time for $g = 3$ and -1.7 ; note that Fig. 5 takes only the minimum values of these curves to avoid the spikes on collisions. The maximum amplitude of the $|3,1\rangle$ and $|4,0\rangle$ components (at least initially) occurs on collisions (corresponding to a minimum amplitude of $|2,2\rangle$). Decreasing of this peak amplitude may be interpreted as the time of collisions between clusters becoming less well defined, due to the distance between their centers of mass becoming less well defined (i.e., its corresponding probability

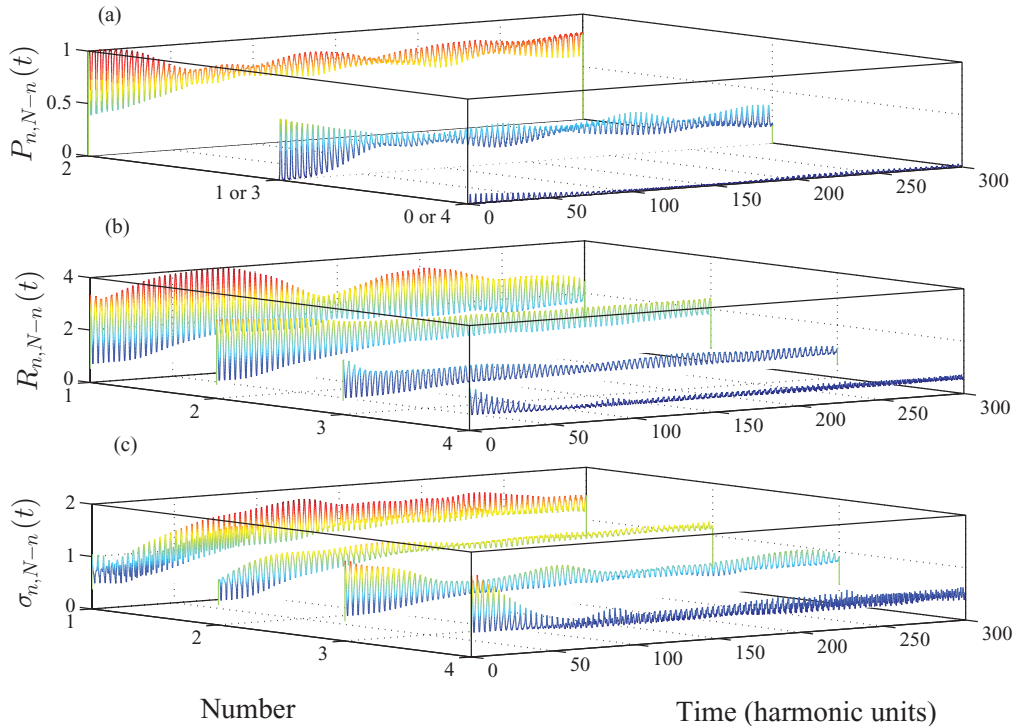


FIG. 6. (Color online) All quantities are in harmonic oscillator units (length is in units of $\sqrt{\hbar/M\omega}$ and time is in units of ω^{-1}). (a) For $g = 3$ and $x_0 = 3$, time evolution of the probability of finding n (or $N - n$) atoms to the right with the amplitudes of wave-function components decomposed into eigenfunctions of the L or R number operator, defined in Eq. (18). (b) Expectation value of the position to the right on sections of wave function decomposed into eigenfunctions of the L or R number operator, defined in Eq. (22). (c) Variance in position to the right as defined in Eq. (23), paralleling (b). The expectation value to the right [(b)] effectively tracks the particlelike motion, but after long times the motion appears effectively damped. (c) can quantify this effect: The peaks of $\sigma_{n,N-n}$ increase from their initial value and continue to oscillate about a maximum, except for $\sigma_{4,0}$ (which is only significantly probable during collisions), indicating a transfer of energy to the degrees of freedom described in Secs. IV B2 and IV B3. This remains true even at very long times $t \sim 1000$, with progressively smaller partial revivals, and so can be said to have equilibrated.

density becomes broader) and the forming of intracluster excitations.

At late times ($t > 100$) in Fig. 7, all the expectation values for $n \neq 2$ are almost the same as those for Gaussians centered on zero. This is due to only the two-dimer (attractive $n = 2$ ground states) setup being significant, as the exciting of intracluster excitations is suppressed by the large energy gap and atom transfer interactions are suppressed by an energy difference, leading to a phase mismatch and hence a cancellation. However, energy is still transferred to the relative position wave function (described in Sec. IV B2), increasing the uncertainty in the separation of dimers, and so some component of the wave function is always undergoing a collision yielding a finite value for the left-right number uncertainty. As a result of our scaling in Eq. (17), the $n \neq 2$ values are just those of the dimer system in collision and only a small contribution to $|3, 1\rangle$ comes from states that are similar to a superposition of a cluster of three atoms to the left (right) and a free atom to the right (left).

C. Equilibration of energy into intercluster and intracluster excited states

We wish to quantify the amount of energy transferred from the center-of-mass energy of each cluster to excitations

between the atoms, as discussed in Secs. IV B2 and IV B3. We therefore study $\sigma_{n,N-n}(t)$, the standard deviation in the position to the right, for a given number of atoms to the right, as defined in Eq. (23). This is essentially the width of the atomic density distribution on the right-hand side, about the expected value for position, given that n atoms are on the right-hand side [defined in Eq. (22)].

These are plotted in Fig. 6(c). The repulsive case shows a consistent increase in the height of the peaks (excepting the $n = 4$ peak), with only small periodic oscillations. The attractive case, however, shows $\sigma_{n,N-n}(t)$ to be initially similar, but then dropping to a minimum value for $n \neq 2$. We note that $\sigma_{n,N-n}(t)$ cuts off anything on the left side and so is difficult to relate to the amount of excitation if the left and right states are separated by a distance smaller than the size of their internal structure, as they will contribute to all the $n \neq 2$ expectation values. Intracluster excitations as we have defined them are present if the wave function on either side of the center does not look like a displaced n -atom ground state; it is possible that such excitations could reduce the position uncertainty, but are generally expected to make it broader and thus increase $\sigma_{n,N-n}(t)$. These excitations are dominant processes in the increasing of σ for the repulsive case plotted in Fig. 6(c) and appear to persist at long times.

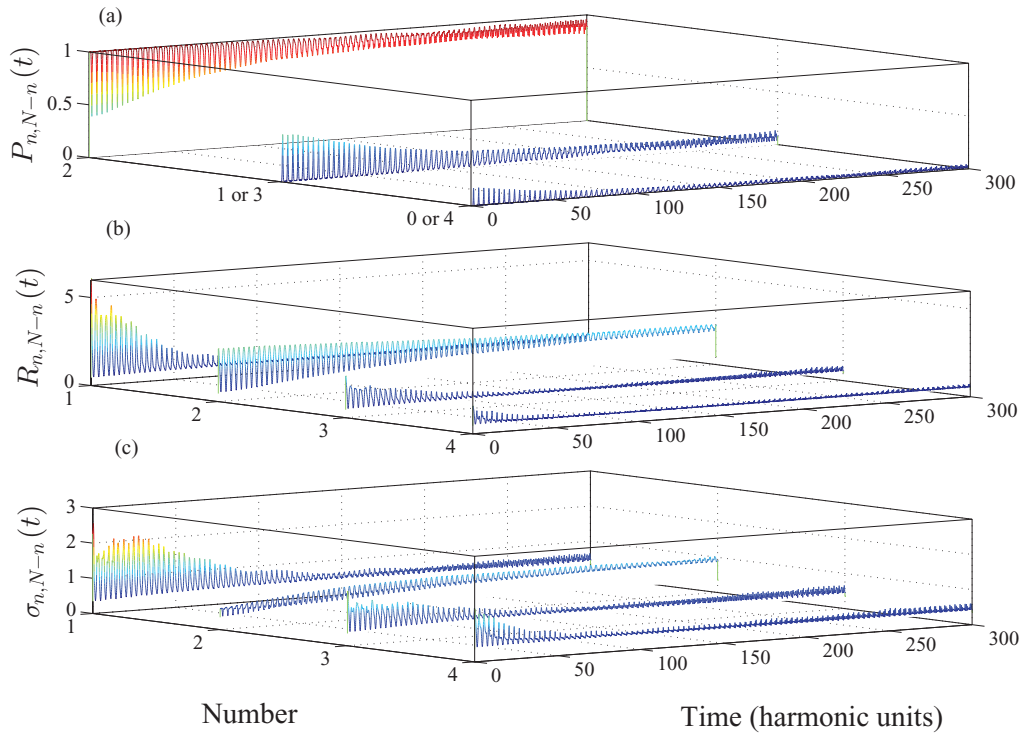


FIG. 7. (Color online) Same quantities as in Fig. 6, but with $g = -1.7$. (a) Probability to find a given left-right number configuration. (b) The short-term behavior of the expected one-atom position is similar to the repulsive case, but is increased in magnitude. At long times, the right-position expectation values drop to an approximately constant value for all but $n = 2$, this being the value of a Gaussian state in the center of the trap, for reasons explained in Sec. VII B. This is also the case in (c): Essentially the only significant contribution to the $n \neq 2$ states comes from uncertainty in the separation of the atomic dimers, which smooths over transfer effects.

For the $g < 0$ case, at very early times, say, $t < 20$, the contribution to $\sigma_{3,1}(t)$ from states in the single-particle and cluster-of-three configuration is visible. By (approximate) momentum conservation, the single atom must have considerably more energy after a collision than the three-atom state, which explains the large $n = 1$ position expectation values away from collision. However, in the strongly attractive case this transfer process is cyclic and it never transfers large populations to these configurations. As we noted before, contributions can come from an oscillating dimer state if the relative separation is small. Initially this only occurs during collision, but intercluster excitations (which can be interpreted as an increased uncertainty in how much the centers of each cluster have shifted due to interactions) lead to an increase in relative position uncertainty.⁶ Hence, at late times there is always significant wave-function density in the trap center, that is to say, at any time $t > t_{\text{late}}$ some non-negligible part of the wave function is always undergoing collision. Hence, if the contribution from the singlet-triplet state is too small to see, we can conclude that the $\sigma_{2,2}(t)$ reaching a maximum corresponds to this mode reaching a steady configuration. This is the dominant effect in the attractive case shown in Fig. 7, but is also present for $g > 0$.

D. Relaxation to equilibrium

One question of interest is whether the system reaches an equilibrium at long times. We attempt to quantify this by looking at the single-body density matrix and its von Neumann entropy, given by Eq. (25); however, this quantity (like most in our system) has a time dependence due to the repeated collisions that are a consequence of the system as a whole being held within a harmonic confining potential. In order to simplify our analysis we look at the time-averaged value over a period of $T = 2\pi$ and quantify the degree of short-time change via the variance of this average. These are plotted in Fig. 8. Figure 8(a) shows that for both positive and negative g , S_{vN} increases towards a maximum value, with small-amplitude oscillations in a similar way to ΔN , but with much smaller variations. For fixed $|g|$, the $g > 0$ entropy generally increases slightly faster and to higher values than the equivalent $g < 0$ case, but is otherwise quite similar. Figure 8(b) shows the standard deviation over the 2π averaging period; the rapidly changing (time scales of less than 2π) effects continue for much longer in the attractive case compared to the repulsive. Transfer effects (discussed in Sec. IV B4) are likely the cause of this short-time oscillation as they are predicted to be cyclic on the time scale of a few collisions when $g \approx 1$. The variation dying down at long times can be explained for the $g > 0$ case by intracluster excited states breaking the cyclic effect and for $g < 0$ by the slower effect of the broadening of the intercluster wave function to the point where the collision time is not well defined.

⁶However, Fig. 5 indicates this process undergoes partial revivals.

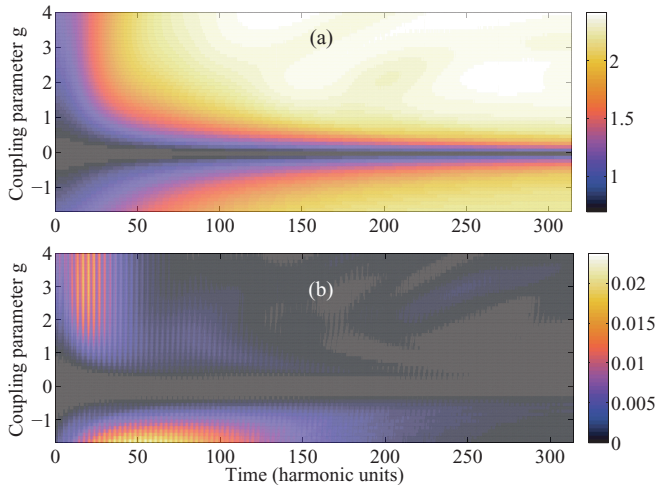


FIG. 8. (Color online) All quantities are in harmonic oscillator units: for $x_0 = 3$, (a) time evolution (measured in units of ω^{-1}) of the von Neumann entropy (averaged over a time period of 2π), as defined by Eqs. (25) and (26), and (b) time evolution of the standard deviation of this quantity, given by the square root of Eq. (27), for a range of interaction strengths both repulsive and attractive. Entropy increases gradually at early times $t < 10\pi$ and then increases at a more rapid rate before leveling off to an almost constant value with small fluctuations. This behavior is similar for both attractive and repulsive interactions. The variance over the 2π averaging range behaves very differently for strong attractive and repulsive interactions, with the short-time-scale fluctuations persisting for much longer if $g < 0$. This difference is explained by a change in the dominant processes, with the attractive system being unable to excite the relative degrees of freedom in a cluster and thus transfer of atoms between each cluster becoming more significant. Figure 6(b) shows that atom transfer dynamics in the repulsive case have only small fluctuations at late times.

VIII. CONCLUSION

We have considered a system of $N = 4$ atoms with contact interactions, confined within in a harmonic potential. Our initial condition was a symmetric setup of two $(N/2)$ -atom ground states, displaced from one another by a distance x_0 (taken to be three harmonic oscillator lengths for most of the numerics), which we then left to oscillate and undergo collisions. Initially there is no entanglement between the atoms on the left and on the right, however, interactions lead to the generation of entanglement.

We investigated left-right number variation within the system, based on an operator that could in principle be measured directly in the experimental setup we suggest in this paper. Initially both (left and right) states have a near-definite number of two atoms and hence a number uncertainty ΔN_R , which is initially close to zero. When the left and right states are well separated, ΔN_R is a measure of entanglement between the left and right sides. However, when the two states are close, i.e., during collisions, $\Delta N_R \sim N/4 = 1$; we therefore investigated the difference from the minimum-to-minimum value taken over a time range of around π , i.e., the minimum value of ΔN_R obtained after the n th collision. There is a marked difference in the evolution of ΔN_R between the $g < 0$ (attractive) and $g > 0$ (repulsive) cases. When $|g| \gtrsim 0.5$, number uncertainty builds

up much more slowly with attractive interactions than with repulsive, essentially resisting entanglement. This is despite a large increase to the change in number uncertainty that is generated by a single collision. This increases quadratically with $|g|$ when $g \lesssim -1.3$, but in the repulsive case the increase reaches a maximum and then drops as g increases further. Additionally, for $g > 0$ we observe long-time-scale high-amplitude number fluctuations, which continue even at late times (over 100 collisions).

This behavior is explained by our time-dependent perturbation theory on the atom transfer process and the energy difference between the intracluster excited states. We investigated the effect of ΔE_{int} , the energy difference in intracluster energies between the $\{2,2\}$ (two displaced $N = 2$ ground states) and $\{3,1\}$ [one free atom and one ($N = 3$)-atom ground state] configurations. Assuming the average interaction energy between the clusters to be weak (i.e., $|Ag| \ll 1$), increases to $|\Delta E_{\text{int}}|$ lead to a phase mismatch and thus to destructive interference so that the population transfer cycles periodically. If intracluster excited states are present, this picture breaks down since each of these excited states phase evolves at a different rate; cancellation becomes more complicated and the states less localized, which occurs for large $g > 0$ at long times. The energy gap between the ground and excited states of each of the $(N/2)$ -atom clusters is increased (decreased) when g gets smaller (larger), which reduces the maximum population that can be transferred to excited states. The excited states become effectively inaccessible as $g \ll 0$, resulting in an effectively two-level system of the $\{2,2\}$ and $\{3,1\}$ configurations. Our perturbation theory indicates that for sufficiently strong attractive interactions, with very specific values, phase matching would be possible, allowing for resonant transfer. However, this is outside the regime our numerical method is capable of reliably portraying and will remain an avenue for future research.

By separating the system into components of the wave function with definite number (number states of the number-to-the-right operator) we have observed the evolution of the positions associated with one-, two-, and three-atom number states and the right-side position variance. For $g = 3$ the peaks in position variance increase to a maximum for all $N_R = n$ in around 100 harmonic time units ($100/2\pi$ oscillator periods or around 30 collisions) and do not fluctuate greatly. Considering instead the case where $g = -1.7$, after 60 collisions, we find that for $N_R \neq 2$ position and position uncertainty are the same as they are for a state undergoing collision, whereas $N_R = 2$ tends to a maximum. This indicates that the state is well described by two atomic dimers with a significant uncertainty in their relative displacement and almost no amplitude of a singlet-trimer-like state is present in the wave function; this motion again undergoes partial revivals on very long time scales.

In addition, we have investigated the von Neumann entropy of the single-body density matrix $S_{\text{vN}}(t)$ in order to investigate to what degree the system tends to an equilibrium. We note that $S_{\text{vN}}(t)$ is zero for a product state (all atoms with the same wave function and occupying the same mode) and can be considered a measure of how mean-field-like the state is. Additionally $S_{\text{vN}}(t)$ is constant for our system if $g = 0$, despite the wave function evolving periodically in time. At long times with

repulsive interactions, S_{vN} (time averaged over a period of 2π) increases to a steady value with only small fluctuations over the averaging period. However, long-term fluctuations (over the order of twenty π time units) are still present and appear to be due to atom transfer processes, which do not appear to equilibrate on the time scales considered in this paper. The time required to reach maximum entropy decreases with larger g , but this appears to saturate with little change for $g \gtrsim 2$; for an initial separation of $x_0 = 3$ this takes around 30 collisions. This short-term increase appears to be due to the intercluster degrees of freedom discussed in the previous paragraph; the associated probability density with the separation of the two clusters becomes less peaked. With very weak attractive interactions, the system's behavior is similar to the repulsive case; however, for $|g| \gtrsim 0.5$, higher intracluster excited states become less accessible, leading effectively to a reduction in the number of accessible degrees of freedom such that the left-right states behave more like solitons. In this case, the time average of $S_{vN}(t)$ does not tend to a long-term mean value as compared with the case of repulsive interactions of similar magnitude; there is also a great deal more short-time variation, which persists for longer. The short-time variation can be attributed to the strong atom transfer effects, which are predicted to cycle population continually due to an energy difference. The effect eventually reduces as displacement uncertainty between the two bound states (which now behave like quantum solitons) increases, which is the mechanism behind the long-term entropy increase.

A pseudoperiodicity effect is also present. The noninteracting system is periodic with a period π and thus the Fourier transform of any time-dependent expectation values will have frequency peaks at n/π . We have examined how these peaks shift for the left-right number uncertainty as interaction strength is varied and have found an approximately linear shift with g over the range considered. Changes to higher-order components of the frequency spectrum depend deviate slightly from the linear dependence shown by the first order, with differences only clearly manifest for $|g| \gtrsim 1$.

ACKNOWLEDGMENTS

We would like to thank the UK EPSRC for funding (Grant No. EP/G056781/1) and the Jack Dodd Centre (S.A.G.) for support, as well as Lincoln D. Carr for illuminating discussions.

APPENDIX A: IDENTITIES INVOLVING JACOBI COORDINATES

1. First identity

We wish to show that the Jacobi coordinates defined by Eqs. (5) and (6) satisfy

$$\sum_{k=1}^N x_k^2 = Nx_{C(N)}^2 + \sum_{k=2}^N \frac{k-1}{k} \xi_k^2. \quad (\text{A1})$$

We prove this inductively. The $N = 2$ case can readily be verified, after which we may consider the increase of number

from $N - 1$ to N . In particular,

$$\sum_{k=1}^N x_k^2 = x_N^2 + (N-1)x_{C(N-1)}^2 + \sum_{k=2}^{N-1} \frac{k-1}{k} \xi_k^2. \quad (\text{A2})$$

Noting that $\xi_N = x_N - x_{C(N-1)}$, we then deduce

$$\begin{aligned} \sum_{k=1}^N x_k^2 &= x_N^2 + (N-1)x_{C(N-1)}^2 \\ &\quad - \frac{N-1}{N} [x_N - x_{C(N-1)}]^2 + \sum_{k=2}^N \frac{k-1}{k} \xi_k^2. \end{aligned} \quad (\text{A3})$$

Collecting terms, this reduces to

$$\begin{aligned} \sum_{k=1}^N x_k^2 &= \frac{1}{N} [x_N + (N-1)x_{C(N-1)}]^2 + \sum_{k=2}^N \frac{k-1}{k} \xi_k^2 \\ &= Nx_{C(N)}^2 + \sum_{k=2}^N \frac{k-1}{k} \xi_k^2, \end{aligned} \quad (\text{A4})$$

which completes the proof. An equivalent result also holds in three dimensions [51].

2. Second identity

We rephrase Eq. (6) as $x_k = \xi_k + [1/(k-1)] \sum_{j=1}^{k-1} x_j$. Recursively substituting in equivalent expressions for $x_{k-1}, x_{k-2}, \dots, x_{N/2+1}$ yields (for $N/2 + 1 < k \leq N$)

$$x_k = \xi_k + \sum_{j=N/2+1}^{k-1} \frac{\xi_j}{j} + \frac{1}{N/2} \sum_{j=1}^{N/2} x_j, \quad (\text{A5})$$

and for $k = N/2 + 1$ we have $x_{N/2+1} = \xi_{N/2+1} + (2/N) \sum_{j=1}^{N/2} x_j$. Hence, summing over all $k \in \{N/2 + 1, N/2 + 2, \dots, N\}$,

$$\begin{aligned} \sum_{k=N/2+1}^N x_k &= \sum_{k=N/2+1}^N \xi_k + \sum_{k=N/2+2}^N \sum_{j=N/2+1}^{k-1} \frac{\xi_j}{j} + \sum_{k=1}^{N/2} x_k \\ &= \sum_{k=N/2+1}^N \xi_k + \sum_{k=N/2+1}^{N-1} \frac{N-k}{k} \xi_k + \sum_{k=1}^{N/2} x_k \\ &= \sum_{k=N/2+1}^N \frac{N}{k} \xi_k + \sum_{k=1}^{N/2} x_k, \end{aligned} \quad (\text{A6})$$

from which we deduce the desired identity

$$\sum_{k=N/2+1}^N x_k - \sum_{k=1}^{N/2} x_k = \sum_{k=N/2+1}^N \frac{N}{k} \xi_k. \quad (\text{A7})$$

APPENDIX B: CALCULATIONS FOR THE NUMBER-TO-THE-RIGHT OPERATOR

1. Analytically determined properties of \hat{N}_R^2

From the definition of Eq. (13) it follows that

$$\hat{N}_R^2 = \int_0^\infty dx dx' \hat{\Psi}^\dagger(x) \hat{\Psi}^\dagger(x') \hat{\Psi}(x) \hat{\Psi}(x') + \hat{N}_R \quad (\text{B1})$$

and, given a general (symmetrized) many-body wave function $\psi(\vec{x})$, one may deduce the expectation values

$$\langle \hat{N}_R \rangle = N \int_0^\infty dx_1 \int_{-\infty}^\infty dx_2 \cdots dx_N |\psi(\vec{x})|^2, \quad (\text{B2})$$

$$\begin{aligned} \langle \hat{N}_R^2 \rangle &= N(N-1) \int_0^\infty dx_1 dx_2 \int_{-\infty}^\infty dx_3 \cdots dx_N |\psi(\vec{x})|^2 \\ &+ \langle \hat{N}_R \rangle. \end{aligned} \quad (\text{B3})$$

For a product-state wave function $\psi(\vec{x}) = \prod_{k=1}^N \phi(x_k)$, expectation values are simple to calculate, as all integrals are separable and most evaluate to unity. In this case

$$\langle \hat{N}_R \rangle = N \int_0^\infty dx |\phi(x)|^2, \quad (\text{B4})$$

$$\begin{aligned} \langle \hat{N}_R^2 \rangle &= N(N-1) \left[\int_0^\infty dx |\phi(x)|^2 \right]^2 + \langle \hat{N}_R \rangle \\ &= [(N-1)/N] \langle \hat{N}_R \rangle^2 + \langle \hat{N}_R \rangle \end{aligned} \quad (\text{B5})$$

and so the variance of \hat{N}_R for a product state simplifies to

$$\Delta_P N_R = \langle \hat{N}_R \rangle (1 - \langle \hat{N}_R \rangle / N). \quad (\text{B6})$$

We may determine analytic expressions when $g = 0$, which, for the purpose of this paper, we limit to the $N = 4$ case. Without interactions, our many-body wave function is given by Eq. (9) and

$$\int_0^\infty dx |\phi(x, \pm x_0, t)|^2 = \frac{1}{2} \{1 \pm \text{erf}[x_0 \cos(t)]\}, \quad (\text{B7})$$

$$\int_{-\infty}^\infty dx \phi^*(x, \pm x_0, t) \phi(x, \mp x_0, t) = e^{-x_0^2 \pm i x_0 \sin(2t)/2}, \quad (\text{B8})$$

$$\begin{aligned} &\int_0^\infty dx \phi^*(x, \pm x_0, t) \phi(x, \mp x_0, t) \\ &= \frac{1}{2} \{1 \pm \text{erf}[x_0 \sin(t)]\} e^{-x_0^2 \pm i x_0 \sin(2t)/2}, \end{aligned} \quad (\text{B9})$$

with erf denoting the error function. Calculating $\langle \hat{N}_R^2 \rangle$ in principle requires accounting for 36 different terms; however, assuming we can neglect terms proportional to $\exp(-2x_0^2)$, only 6 are important and we have

$$\begin{aligned} \langle \hat{N}_R^2 \rangle &\approx \frac{N(N-1)}{24} \{ (1 - \text{erf}[x_0 \cos(t)])^2 \\ &+ 4\{1 - \text{erf}^2[x_0 \cos(t)]\} \\ &+ \{1 + \text{erf}[x_0 \cos(t)]\}^2 \} + \langle \hat{N}_R \rangle \\ &= 5 - \text{erf}^2[x_0 \cos(t)]. \end{aligned} \quad (\text{B10})$$

Subtracting 4 then yields the variance as given by Eq. (16).

2. Numerical calculation of number variance

In order to calculate the number variance we decompose the field operator into our basis set $\hat{\Psi}(x) = \sum_k \hat{a}_k \phi_k(x)$. In this form we can express \hat{N}_R^2 as

$$\hat{N}_R^2 = \sum_{i,j,k,\ell} y_{ik} y_{j\ell} \hat{a}_i^\dagger \hat{a}_j^\dagger \hat{a}_k \hat{a}_\ell + \hat{N}_R, \quad (\text{B11})$$

where $y_{j\ell} = \int_0^\infty dx \phi_j(x) \phi_\ell(x)$ is the positive space overlap between two Hermite functions, given by $\delta_{j\ell}/2$ if $j + \ell$ is even

and otherwise given by

$$\begin{aligned} y_{j\ell} &= (-1)^{(j+\ell-1)/2} {}_2F_1(-j, 1 - [j - \ell]/2; 1 - [j + \ell]/2, -1) \\ &\times \frac{2^{-j}(j + \ell + 2)!!}{\sqrt{2\pi j! \ell!}}, \end{aligned} \quad (\text{B12})$$

where ${}_2F_1$ denotes a standard hypergeometric function. Likewise, the integral from minus infinity to zero is $(-1)^{j+\ell} y_{j\ell}$. This formula is useful for small numbers and testing, but for practical purposes we calculate the integral via Gauss-Laguerre quadrature, which is numerically exact for odd $j + \ell$ (all other cases are trivially zero or one-half) given a rule of order $(j + \ell + 1)/2$ or higher. Given our truncated basis and symmetry about $x = 0$, this can be expressed as a finite-size matrix of only even-parity functions with $\langle \hat{N}_R \rangle = N/2$ just a numerical constant for our initial condition.

3. Numerical calculation of restricted region expectation values

In addition to this we wish to calculate expectation values in restricted regions via Eq. (17), corresponding to sections of the wave function with exactly n particles to the left or right, along with the associated normalization factors when the wave function is divided into these regions. If our many-body wave function is $\psi(\vec{x})$, then the normalization factors are given by

$$\mathcal{N}_n = \frac{N!}{(N-n)!n!} \int_0^\infty dx_1 \cdots dx_n \int_{-\infty}^0 dx_{n+1} \cdots dx_N |\psi(\vec{x})|^2 \quad (\text{B13})$$

and the expectation value of the distance-to-the-right operator [defined in Eq. (21)] is equal to

$$\begin{aligned} \langle \hat{x}_R^{(n)} \rangle &= \mathcal{N}_n^{-1} \int_{-\infty}^\infty dx_1 \cdots dx_N \sum_{k=0}^N x_k \theta(x_k) \\ &\times \sum_{\mathcal{P}} \prod_{k=1}^n \Theta(x_k) \prod_{j=n+1}^N \Theta(-x_j) |\psi(\vec{x})|^2 \\ &= \mathcal{N}_n^{-1} \frac{N!}{(N-n)!n!} \int_0^\infty dx_1 \cdots dx_n \\ &\times \int_{-\infty}^0 dx_{n+1} \cdots dx_N \sum_{k=n+1}^N x_k |\psi(\vec{x})|^2. \end{aligned} \quad (\text{B14})$$

For computation, these operators are converted into matrix form by taking the matrix elements between different elements of the basis set and then projected to our reduced (center-of-mass ground-state) basis.

APPENDIX C: TWO-CLUSTER WAVE-FUNCTION EVOLUTION

Here we derive the time-dependent wave function describing the center of masses of our two-cluster system, i.e., the part acted on by $\hat{H}_{L/R}^{(C)}$, the center-of-mass components from Eq. (28), with \hat{H}_I ignored. Denoting y_1, y_2 as the coordinates of the center of masses of each cluster, up to a normalization

factor our initial two-cluster wave function is given by

$$\begin{aligned} \langle y_1, y_2 | \varphi_{n, N-n}(0) \rangle &\propto \exp\left(-\frac{N-n}{2} \left[y_2 + \frac{nX_n}{N-n} \right]^2\right) \\ &\times \exp\left(-\frac{n}{2} [y_1 - X_n]^2\right) + \mathcal{T}_{\text{perm}}, \end{aligned} \quad (\text{C1})$$

with $\mathcal{T}_{\text{perm}}$ indicating the term obtained by permuting y_1 and y_2 , as required by symmetry. This gives rise to a time-dependent normalization constant, which we do not discuss here. If we instead express this in terms of $y_C = [ny_1 + (N-n)y_2]/N$ and $y_R = y_1 - y_2$ we have

$$\begin{aligned} \langle y_C, y_R | \varphi_{n, N-n}(0) \rangle &\propto \exp\left(-\frac{n[(N-n)y_R - NX_n]^2}{2N[N-n]}\right) \\ &\times \exp\left(-\frac{Ny_C^2}{2}\right) + \mathcal{T}_{\text{perm}}, \end{aligned} \quad (\text{C2})$$

where in this case $\mathcal{T}_{\text{perm}}$ is simply flipping the sign of y_R and we can factor out the y_C dependence. If we temporarily ignore interactions between the two clusters, it is straightforward to generalize this to the time-dependent case via Eq. (10):

$$\begin{aligned} \langle y_C, y_R | \varphi_{n, N-n}(t) \rangle &\propto \exp\left(-\frac{n[(N-n)y_R - NX_n \cos(t)]^2}{2N[N-n]}\right) \\ &\times \exp\left(-\frac{Ny_C^2}{2}\right) \exp\left\{i\left[t - ny_R X_n \sin(t) \right. \right. \\ &\left. \left. + \frac{X_n}{4} \left(n - \frac{n}{N-n}\right) \sin(2t)\right]\right\} + \mathcal{T}_{\text{perm}}. \end{aligned} \quad (\text{C3})$$

Interactions between clusters can modify only the y_R -dependent part of this wave function.

APPENDIX D: ENERGY BOUND FOR HAMILTONIAN VARIANCE

As the Hamiltonian is time independent, the time-evolution operator commutes with all powers of the Hamiltonian. Denoting our state as $|\psi(t)\rangle$, we have for any time t

$$\langle \psi(t) | \hat{H}^n | \psi(t) \rangle = \langle \psi(0) | \hat{H}^n | \psi(0) \rangle, \quad n = 1, 2, \dots \quad (\text{D1})$$

As absolute values of energy are not physically important, we consider a rezeroed Hamiltonian

$$\hat{\mathcal{H}} = \hat{H} - \langle \psi(0) | \hat{H} | \psi(0) \rangle \quad (\text{D2})$$

as it will make the mathematics more convenient. Introducing the notation for the variance of the rezeroed Hamiltonian

$$\Delta E^2 = \langle \hat{\mathcal{H}}^2 \rangle, \quad (\text{D3})$$

we note that this quantity must be positive and real as \hat{H} is a Hermitian operator.

Let us define two wave functions $|\psi_1(t)\rangle$ and $|\psi_2(t)\rangle$ as being negligibly mixed at a certain point in time if

$$\langle \psi_1(t) | \hat{\mathcal{H}}^n | \psi_2(t) \rangle \leq \eta, \quad n = 1, 2, \quad (\text{D4})$$

with η a small parameter. Note that in lattice models η could be exactly zero up to some finite power n . If both the initial wave function and $|\psi_{1,2}(t)\rangle$ are normalized to one and the latter are negligibly mixed, the wave function at time t can be written

(up to a global phase factor) as

$$|\psi(t)\rangle = \sqrt{p} |\psi_1(t)\rangle + \sqrt{1-p} e^{i\alpha} |\psi_2(t)\rangle, \quad (\text{D5})$$

with real α and $0 \leq p \leq 1$. Introducing the notation

$$\langle \hat{\mathcal{H}}^n \rangle_j \equiv \langle \psi_j(t) | \hat{\mathcal{H}}^n | \psi_j(t) \rangle, \quad (\text{D6})$$

we can see from Eq. (D4) and the fact that the expectation value of total Hamiltonian is zero that these two quantities are related via

$$\langle \hat{\mathcal{H}} \rangle_1 = \frac{p-1}{p} \langle \hat{\mathcal{H}} \rangle_2 + O(\eta). \quad (\text{D7})$$

Setting $\eta = 0$ in Eq. (D4), we have for $n = 2$

$$\begin{aligned} \Delta E^2 &= p \langle \hat{\mathcal{H}}^2 \rangle_1 + (1-p) \langle \hat{\mathcal{H}}^2 \rangle_2 \\ &\geq p \langle \hat{\mathcal{H}} \rangle_1^2 + (1-p) \langle \hat{\mathcal{H}} \rangle_2^2, \end{aligned} \quad (\text{D8})$$

with the second step true again by the fact that \hat{H} is Hermitian. Finally, substituting in for $\langle \hat{\mathcal{H}} \rangle_1$ via Eq. (D7), we obtain

$$\Delta E^2 \geq \frac{1-p}{p} \langle \hat{\mathcal{H}} \rangle_2^2, \quad (\text{D9})$$

$$\Delta E^2 \geq \frac{p}{1-p} \langle \hat{\mathcal{H}} \rangle_1^2, \quad (\text{D10})$$

$$\Delta E^2 \geq \frac{(\langle \hat{\mathcal{H}} \rangle_1 - \langle \hat{\mathcal{H}} \rangle_2)^2}{p(1-p)}, \quad (\text{D11})$$

which leads to Eq. (45) in the main text.

1. Analytic calculations of ΔE

For our two-particle initial condition, if $x_0 \gg 1$, i.e., well-separated initial clusters, we can analytically determine E and ΔE . Within this well-separated approximation we only need to consider one cluster, displaced a distance x_0 from the center, and multiply by 2 to get the values for the whole wave function. For dimers, our wave function is $f(x_1 - x_0, x_2 - x_0)^{(2)}$ as defined in Eq. (11); otherwise it is not analytic. This wave function is still an eigenstate of the relative Hamiltonian (for n particles), with some eigenvalue $E_{\text{rel}}^{(n)}$, but not of the center-of-mass part. Therefore, we need only consider the center-of-mass Hamiltonian

$$H_C(x_C) = -\frac{1}{2n} \frac{\partial^2}{\partial x_C^2} + \frac{nx_C^2}{2} \quad (\text{D12})$$

acting on the displaced ground state

$$\psi_C(x_C) = \left(\frac{n}{\pi}\right)^{1/4} \exp(-n[x_C - x_0]/2) \quad (\text{D13})$$

to get all contributions to the variance. Applying the Hamiltonian to this wavefunction, we obtain

$$\begin{aligned} H_C \psi_C(x_C) &= \left(\frac{1}{2} + nx_0 x + \frac{nx_0^2}{2}\right) \psi_C(x_C), \\ H_C^2 \psi_C(x_C) &= \left[\frac{1}{4} + \frac{nx_0}{2} (4x - 3x_0) + n^2 x_0^2 (x_0 - 2x)^2\right] \\ &\times \psi_C(x_C), \end{aligned} \quad (\text{D14})$$

which can then be used to determine the expectation values

$$\langle \hat{H}_C \rangle = \frac{1}{2} + \frac{nx_0^2}{2}, \quad \langle \hat{H}_C^2 \rangle = \frac{1}{4} + nx_0^2 + \frac{n^2 x_0^4}{4}. \quad (\text{D15})$$

Then ΔE can be calculated as the standard deviation of two times \hat{H}_C ,

$$\Delta E = 2\sqrt{\langle \hat{H}_C^2 \rangle - \langle \hat{H}_C \rangle^2} = \sqrt{2n}x_0, \quad (\text{D16})$$

which is twice the square root of the difference between the initial (dimensionless) potential energy and the ground-state

energy. The reasons for this are similar to why a classical coherent state with an average value of N photons has a shot noise proportional to $N^{1/2}$. Note that this result relies on $\exp(-nx_0^2) \ll 1$ and so can only be considered valid to this order.

-
- [1] M. H. Anderson, J. R. Ensher, M. R. Matthews, C. E. Wieman, and E. A. Cornell, *Science* **269**, 198 (1995).
- [2] K. B. Davis, M. O. Mewes, M. R. Andrews, N. J. van Druten, D. S. Durfee, D. M. Kurn, and W. Ketterle, *Phys. Rev. Lett.* **75**, 3969 (1995).
- [3] I. Bloch, *Nat. Phys.* **1**, 23 (2005).
- [4] T. Schumm, S. Hofferberth, L. M. Andersson, S. Wildermuth, S. Groth, I. Bar-Joseph, J. Schmiedmayer, and P. Krüger, *Nat. Phys.* **1**, 57 (2005).
- [5] C. Ryu, M. F. Andersen, A. Vaziri, M. B. d'Arcy, J. M. Grossman, K. Helmerson, and W. D. Phillips, *Phys. Rev. Lett.* **96**, 160403 (2006).
- [6] R. V. Mishmash and L. D. Carr, *Phys. Rev. Lett.* **103**, 140403 (2009).
- [7] S. Sinha, A. Y. Cherny, D. Kovrizhin, and J. Brand, *Phys. Rev. Lett.* **96**, 030406 (2006).
- [8] C. C. Bradley, C. A. Sackett, and R. G. Hulet, *Phys. Rev. Lett.* **78**, 985 (1997).
- [9] L. Khaykovich, F. Schreck, G. Ferrari, T. Bourdel, J. Cubizolles, L. D. Carr, Y. Castin, and C. Salomon, *Science* **296**, 1290 (2002).
- [10] K. E. Strecker, G. B. Partridge, A. G. Truscott, and R. G. Hulet, *Nature (London)* **417**, 150 (2002).
- [11] R. J. Dodd, M. Edwards, C. J. Williams, C. W. Clark, M. J. Holland, P. A. Ruprecht, and K. Burnett, *Phys. Rev. A* **54**, 661 (1996).
- [12] S. L. Cornish, S. T. Thompson, and C. E. Wieman, *Phys. Rev. Lett.* **96**, 170401 (2006).
- [13] T. P. Billam, S. A. Wrathmall, and S. A. Gardiner, *Phys. Rev. A* **85**, 013627 (2012).
- [14] N. G. Parker, S. L. Cornish, C. S. Adams, and A. M. Martin, *J. Phys. B* **40**, 3127 (2007).
- [15] A. D. Martin, C. S. Adams, and S. A. Gardiner, *Phys. Rev. A* **77**, 013620 (2008).
- [16] L. Salasnich, A. Parola, and L. Reatto, *Phys. Rev. A* **65**, 043614 (2002).
- [17] J. Cuevas, P. G. Kevrekidis, B. A. Malomed, P. Dyke, and R. G. Hulet, [arXiv:1301.3959](https://arxiv.org/abs/1301.3959) [cond-mat.quant-gas].
- [18] B. Eiermann, T. Anker, M. Albiez, M. Taglieber, P. Treutlein, K.-P. Marzlin, and M. K. Oberthaler, *Phys. Rev. Lett.* **92**, 230401 (2004).
- [19] I. B. Spielman, W. D. Phillips, and J. V. Porto, *Phys. Rev. Lett.* **98**, 080404 (2007).
- [20] C. F. Wildfeuer, A. P. Lund, and J. P. Dowling, *Phys. Rev. A* **76**, 052101 (2007).
- [21] B. Lucke, M. Scherer, J. Kruse, L. Pezze, F. Deuretzbacher, P. Hyllus, O. Topic, J. Peise, W. Ertmer, J. Arlt, L. Santos, A. Smerzi, and C. Klempt, *Science* **334**, 773 (2011).
- [22] B. Gertjerenken and C. Weiss, *J. Phys. B* **45**, 165301 (2012).
- [23] B. Gertjerenken, T. P. Billam, L. Khaykovich, and C. Weiss, *Phys. Rev. A* **86**, 033608 (2012).
- [24] A. L. Marchant, T. P. Billam, T. P. Wiles, M. M. H. Yu, S. A. Gardiner, and S. L. Cornish, [arXiv:1301.5759](https://arxiv.org/abs/1301.5759).
- [25] F. Serwane, G. Zürn, T. Lompe, T. B. Ottenstein, A. N. Wenz, and S. Jochim, *Science* **332**, 336 (2011).
- [26] G. Zürn, F. Serwane, T. Lompe, A. N. Wenz, M. G. Ries, J. E. Bohn, and S. Jochim, *Phys. Rev. Lett.* **108**, 075303 (2012).
- [27] M. Cramer, C. M. Dawson, J. Eisert, and T. J. Osborne, *Phys. Rev. Lett.* **100**, 030602 (2008).
- [28] C. Gogolin, M. P. Müller, and J. Eisert, *Phys. Rev. Lett.* **106**, 040401 (2011).
- [29] M. Greiner, O. Mandel, T. W. Hansch, and I. Bloch, *Nature (London)* **419**, 51 (2009).
- [30] F. Benatti, R. Floreanini, and U. Marzolino, *Phys. Rev. A* **85**, 042329 (2012).
- [31] E. H. Lieb and W. Liniger, *Phys. Rev.* **130**, 1605 (1963).
- [32] D. I. H. Holdaway, C. Weiss, and S. A. Gardiner, *Phys. Rev. A* **85**, 053618 (2012).
- [33] J. B. McGuire, *J. Math. Phys.* **5**, 622 (1964).
- [34] L. Pitaevskii and S. Stringari, *Bose-Einstein Condensation* (Oxford Science, Oxford, 2003).
- [35] M. Olshanii, *Phys. Rev. Lett.* **81**, 938 (1998).
- [36] M. Bonitz, K. Balzer, and R. van Leeuwen, *Phys. Rev. B* **76**, 045341 (2007).
- [37] D. T. Pegg and S. M. Barnett, *J. Mod. Opt.* **44**, 225 (1997).
- [38] C. Gerry and P. Knight, *Introductory Quantum Optics* (Cambridge University Press, Cambridge, 2004).
- [39] T. Busch, B. G. Englert, K. Rzążewski, and M. Wilkens, *Found. Phys.* **28**, 549 (1998).
- [40] T. Sowiński, M. Brewczyk, M. Gajda, and K. Rzążewski, *Phys. Rev. A* **82**, 053631 (2010).
- [41] V. V. Sokolov, B. A. Brown, and V. Zelevinsky, *Phys. Rev. E* **58**, 56 (1998).
- [42] T. P. Billam and S. A. Gardiner, *New J. Phys.* **14**, 013038 (2012).
- [43] T. P. Billam, P. Mason, and S. A. Gardiner, *Phys. Rev. A* **87**, 033628 (2013).
- [44] M. Lewenstein and B. A. Malomed, *New J. Phys.* **11**, 113014 (2009).
- [45] M. D. Girardeau, E. M. Wright, and J. M. Triscari, *Phys. Rev. A* **63**, 033601 (2001).
- [46] J. Sebby-Strabley, M. Anderlini, P. S. Jessen, and J. V. Porto, *Phys. Rev. A* **73**, 033605 (2006).
- [47] I. Bloch, J. Dalibard, and S. Nascimbène, *Nat. Phys.* **8**, 267 (2012).
- [48] J. F. Sherson, C. Weitenberg, M. Endres, M. Cheneau, I. Bloch, and S. Kuhr, *Nature (London)* **467**, 68 (2010).
- [49] K. Sun, W. V. Liu, A. Hemmerich, and S. Das Sarma, *Nat. Phys.* **8**, 67 (2012).
- [50] C. Chin, V. Vuletić, A. J. Kerman, S. Chu, E. Tiesinga, P. J. Leo, and C. J. Williams, *Phys. Rev. A* **70**, 032701 (2004).
- [51] T. Yamada, Y. Funaki, H. Horiuchi, G. Röpke, P. Schuck, and A. Tohsaki, *Phys. Rev. C* **79**, 054314 (2009).